AD-A072 841 STATE UNIV OF NEW YORK AT STONY BROOK F/G 11/6
THE RESPONSE OF COATED STEELS TO CAVITATION IN CORROSIVE ENVIRO--ETC(U)
MAR 79 H HERMAN, C R CLAYTON, M DORFMAN N00014-75-C-1018

UNCLASSIFIED TR-4 NL

1 OF 1
AD A072841

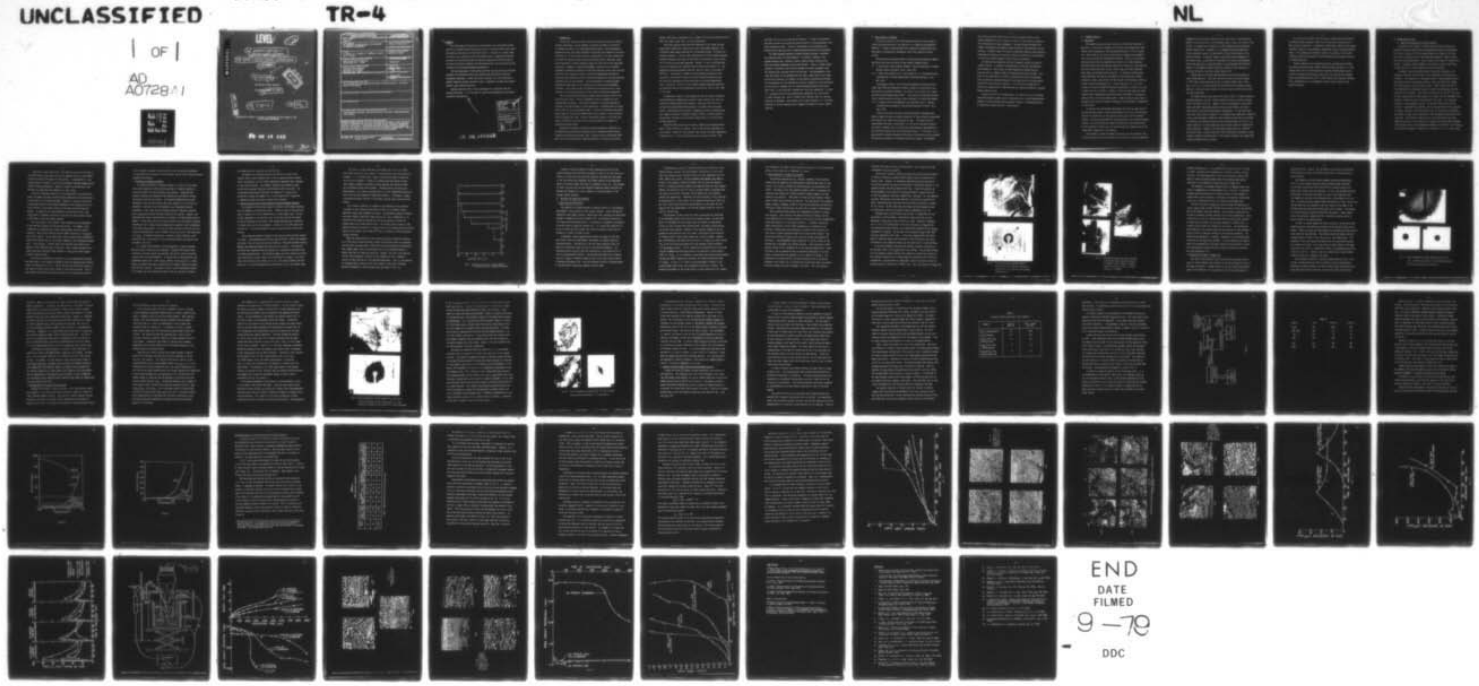

END
DATE FILMED
9-79
DDC

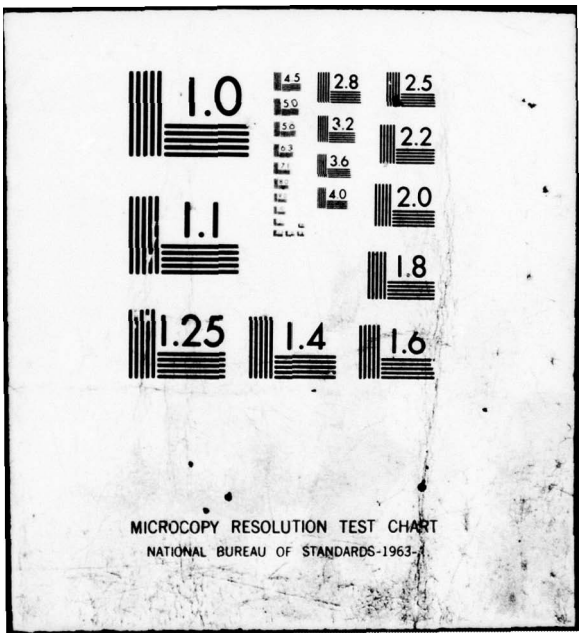
1.0
1.1
1.25
1.4
1.6
1.8
2.0
2.2
2.5
2.8
3.2
3.6
4.0
4.5
5.0
5.6
MICROCOPY RESOLUTION TEST CHART
NATIONAL BUREAU OF STANDARDS-1963-A

AD A072841

LEVEL II

B.S. 2

THE RESPONSE OF COATED STEELS TO CAVITATION IN CORROSIVE ENVIRONMENTS

H./Herman, C.R./Clayton, M./Dorfman, S./Safai, J./Vargas

Mar[illegible]79

A047472

DDC
AUG 13 1979
C

Technical Report No. 4

to

The Office of Naval Research

Contract No. N00014-75-C-1018

DDC FILE COPY

TR-4

64 p.

Reproduction in whole or in part is permitted for any purpose of the United States Government

79 08 10 055

256944

SECURITY CLASSIFICATION OF THIS PAGE (When Data Entered)

REPORT DOCUMENTATION PAGE

READ INSTRUCTIONS BEFORE COMPLETING FORM

1. REPORT NUMBER: SUSB-79-1	2. GOVT ACCESSION NO.
3. RECIPIENT'S CATALOG NUMBER	
4. TITLE (and Subtitle): THE RESPONSE OF COATED STEELS TO CAVITATION IN CORROSIVE ENVIRONMENTS	5. TYPE OF REPORT & PERIOD COVERED: Technical Report No. 4
6. PERFORMING ORG. REPORT NUMBER	
7. AUTHOR(s): H. Herman, C.R. Clayton, M. Dorfman, S. Safai and J. Vargas	8. CONTRACT OR GRANT NUMBER(s): N00014-75-C-1018
9. PERFORMING ORGANIZATION NAME AND ADDRESS: State University of New York, Stony Brook, N.Y. 11794	10. PROGRAM ELEMENT, PROJECT, TASK AREA & WORK UNIT NUMBERS: NR 036-110
11. CONTROLLING OFFICE NAME AND ADDRESS: Office of Naval Research, Department of the Navy, Arlington, VA. 22217	12. REPORT DATE: March, 1979
	13. NUMBER OF PAGES: 61
14. MONITORING AGENCY NAME & ADDRESS(if different from Controlling Office)	15. SECURITY CLASS. (of this report): UNCLASSIFIED
	15a. DECLASSIFICATION/DOWNGRADING SCHEDULE

16. DISTRIBUTION STATEMENT (of this Report)

This document has been approved for public release and sale; Its distribution is unlimited.

17. DISTRIBUTION STATEMENT (of the abstract entered in Block 20, if different from Report)

18. SUPPLEMENTARY NOTES

19. KEY WORDS (Continue on reverse side if necessary and identify by block number)

Flame Spraying, Coatings, Cavitation-Erosion, Corrosion, Aluminum Coating, Zinc Coating.

20. ABSTRACT (Continue on reverse side if necessary and identify by block number)

Thermal-sprayed aluminum, zinc and zinc-aluminum coatings on steel are being studied to determine the resistance afforded by this coating to cavitation-erosion in salt water. Both oxide and metal coatings are being examined to ascertain the details of microstructure of the thermal sprayed layers. NDE of coatings using acoustic emission is currently being evaluated.

DD FORM 1 JAN 73 1473 EDITION OF 1 NOV 65 IS OBSOLETE
S/N 0102-LF-014-6601

UNCLASSIFIED
SECURITY CLASSIFICATION OF THIS PAGE (When Data Entered)

ABSTRACT

This ONR-supported program has concentrated on the cavitation-erosion behavior of thermal-sprayed coatings on steel in distilled and in salt water. The coatings have been Zn, Al and Zn-15 w/o Al. Porosity is a major cause of failure in a cavitation field, and further work is proposed whereby the porosity can be controlled and the coatings examined both from the points of view of corrosion (visually and electrochemically) and cavitation-erosion (visually and with weight-change measurements).

The microstructures of both oxide and metal coatings have been examined through x-ray diffraction and using scanning and transmission electron microscopy techniques. Aside from active coatings, it is also desired to examine thermally-sprayed stainless steels, exothermic coatings and sprayed metallic glass forming materials.

Acoustic emission (AE) is being developed as an important tool for coating evaluation. It is one goal to relate AE measurements to cavitation-corrosion survivability.

Accession For
NTIS GRA&I
DDC TAB
Unannounced
Justification
By
Distribution/
Availability Codes
Dist | Avail and/or special
A

79 08 10 055

I INTRODUCTION

Protective coatings have been applied to metals and alloys by thermal spraying techniques for many decades to provide resistance to corrosion. In engineering tests, zinc and aluminum-coated steels, with and without a polymer top-coat, have been subjected to salt water and industrial corrosion conditions of 12 and 19 years duration, respectively (1,2) and, despite the fact that the coatings always contain some porosity and, therefore, would not be expected to provide complete protection, they have proven remarkably successful. However, in marine environments, structures are frequently subjected to mechanical erosion by cavitation processes and by sand particles. The aim of this program has been to relate the degradation processes of corrosion and cavitation-erosion in marine environments to the microstructure characteristics of the coatings. The microstructure of thermal-sprayed coatings has been shown in this program to be highly process-dependent. Therefore, it has been our goal to examine the microstructure of a range of metallic and oxide coatings and relate these to protective properties.

The cavitation-erosion has been studied using an acoustic horn in distilled and salt water. Surface topography as well as weight-loss were followed during exposure. The corrosion behavior of sprayed coatings of aluminum, zinc and Zn-15wt%. Al were examined by a standard ASTM salt spray test as well as by electrochemical means. There has furthermore been developed a means of carrying out potentiometric measurements of the cavitation-erosion coatings and, thus, using an interruption method, it has been possible to follow the evolution of the corrosion potential attendant to cavitation-erosion attack.

Related to the above corrosion and surface mechanical properties are the detailed microstructural characteristics of thermal-sprayed coatings. Transmission electron microscopy (TEM), scanning electron microscopy (SEM) and x-ray diffraction analysis have been employed to resolve the relation

between spray-process parameters (e.g., powder and wire spray characteristics, feed rate, gases, power level, surface preparation).

The spray processes which have been employed in this study include, oxyacetylene flame torch, electric-arc spray, and plasma spraying. The differences among these processes will be discussed below. Of central importance, however, is the fact that contained within the as-sprayed layered platelett-structure are grains of the order of one micron in size, the details of which we have been examining. Overall, it can be concluded that we are here dealing with a material that has been splat-cooled, i.e., has undergone ultrarapid quenching from the liquid at rates of the order of 10^6°C/sec. This process is known to yield extremely metastable microstructures, which have the asset of having interesting properties and the liability frequently of being non-stable at elevated temperatures (e.g. in service). We have in this research program addressed ourselves to a detailed study of such metastable microstructures and to their stability in-use.

An additional aspect of this program has been post-spray treatments using mechanically-induced pore closing in metal coatings and laser processing of plasma-sprayed oxide coatings. Described here-in will be corrosion and cavitation-erosion behavior of coatings which have been rolled. Shot-peening will be used in subsequent studies to determine how this commercial process influences coating lifetime - we have reason to believe that lifetimes will be greatly enhanced due to this post-spray surface processing.

Non-destructive evaluation of coating integrity and expected performance is most difficult to achieve. Most of the current techniques are not reliable. During the last contract year we have initiated cooperative studies with Dr. K. Ono of UCLA on the use of acoustic emission (AE)

techniques for observing oxide coating behavior. A number of experiments have been carried out to ascertain various apsects of noise generation from oxide coatings on steel. This will be detailed in the following, and further work in the use of AE in coating chracterization will be outlined.

This ONR-supported program on thermal-sprayed coatings is pointing out important areas of future research. The defects inherent in the sprayed coatings (eg., porosity, cracks, rough coatings surface) arise from the processes employed to form the coatings. Clearly, a better understanding is required of the relation between the process parameters and the imperfections contained within the coatings. The measurements of the sizes and extent of the imperfections have been a major part of our study. Porosity and cracking, for example, can be readily controlled by alloying. The AE phenomena are also effected by alloying, leading us to the conclusion that AE can be a valuable tool for coating characterization and testing. Other tests, to be discussed, correlate well with this contention. In fact, it is suggested that the very imperfections themselves (eg. microcracks in oxide coatings) can lead to "plastic-like" behavior when the coatings substrate is deformed. Such concepts can be used to explain the surprising viability of various coatings and to suggest the design of "tough" ceramic coatings.

II BRIEF REVIEW OF PROGRESS

Since the inception of this ONR-supported program we have sought to relate the microstructure of the coating to its chemical and mechanical behavior. A number of publications have resulted and presentations have been made at international conferences which have reported on these results.

Microstructural characterization of plasma-sprayed coatings of metals and alloys have been the topics of two recently awarded theses:

i) V. Wilms (now at MTU, Munich, Germany), "The Microstructure of Plasma Sprayed Ceramic Coatings", Ph.D., June, 1978.

ii) S. Safai (now at Metco, Inc., Long Island, N. Y.), "A Microstructural Investigation of Plasma-Sprayed Metal and Oxide Coatings", Ph.D., May, 1979.

In the above studies, x-ray diffraction methods and electron microscopy (TEM, SEM) were employed to develop a model of solidification and the resulting interfacial bonding. The results point clearly to a "mechanically-assisted metallurgical bond". These ideas were developed further in our cavitation-erosion studies, which resulted in an additional thesis:

iii) J. Vargas (now at Pratt-Whitney, East Hartford, Conn.), "Thermal-Sprayed Active Coatings for the Marine Protection of Steel", M.S., May, 1979.

In this work, both salt spray and potentiokinetic techniques were used to examine the marine corrosion behavior of flame sprayed (oxyacetylene and electric-arc) light alloy coatings on steel. The major thrust in recent months has been a continuation of this work by graduate research assistant M. Dorfman, who is carrying out electrochemical measurements in the cavitation-erosion cell on an interruption basis. In this way, it is now possible to examine dynamically the decay ofthe coating and to ascertain the protective character of different protective systems. Furthermore,

post-spraying coating modification can have a dramatic effect on the dynamic degradation of such systems, and work is continuing on evaluating the effectiveness of these treatments. The modification performed here ranges from mechanically-induced closure (pressing, shot-peening) to laser treating. Polymeric pore-filling has an important effect on both corrosion and mechanical behavior, but not all fillers are effective, and evaluation of the relative effectiveness of the fillers is continuing.

Non-destructive evaluation of thermal-sprayed coatings has been extremely limited. In recently initiated work, carried out cooperatively with Professor K. Ono of UCLA, we have attempted to develop Acoustic Emission (AE) as a method of NDE for plasma-sprayed oxide coatings. This work will be continued in an effort to characterize the noise eminating from a deformed or heated coating and relate that noise to coating and/or interfacial microstructural features. It will be our ultimate goal in this work to develop AE as a NDE technique for coating evaluation, a greatly needed industrial tool.

Further work will be outlined below. The central thrust of this ONR-supported program has been, and will continue to be, a much needed detailed analysis of coating microstructire and how lifetime is influenced and can be improved by controlling this microstructure.

III THERMAL SPRAYING

A. Background

The thermal spraying process involves the continuous injection of materials in the form of a powder or wire into a high temperature flame formed by the combustion of fuel gas-oxygen mixtures, or into a plasma arc. More recently, the use of an electric-arc between two consumable wires has also received considerable attention. (Much of the corrosion work carried out here has been done on electric-arc-formed coatings). The molten particles are propelled towards the surface by a high velocity gas, with velocities close to sonic, where they are rapidly quenched upon impact and thereby form the coating. In industrial applications, these techniques are used for the deposition and protective coatings of metals, oxides, and carbides for the purpose of reclamation, hard surfacing, corrosion protection, etc. Light alloys (eg., Al, Zn, Zn-Al alloys) are usually sprayed with either oxyacetylene or electric arc guns at feed rates up to 50 kg/hr. However, oxides and other materials which require higher temperatures and non-oxidizing environments are generally applied with an inert-gas plasma system. These coatings usually range in thickness from 100 μm to several millimeters and are nominally categorized as thick films.

In spite of the considerable development work that has gone into improving the spray process, there unfortunately still exists limited appreciation for the details of the microstructural aspects of the sprayed coating. The major technologically related aspects of the sprayed coatings include: (i) coating-substrate adhesion mechanism(s) and characteristics of the interfacial region; and (ii) particle-particle cohesion and the related "bulk" properties of the coating.

With respect to adhesion between the coating and the substrate, the first molten particles which impinge onto the surface, usually cleaned and

roughened by grit blasting, experience very rapid rates of solidification. However, the cooling rate in the subsequent layers, within the "bulk" of the coating, is lowered by an increase in surface temperature and decreasing thermal conductivity. Therefore, it is probable that the differential cooling mechanism results in nonuniformity of the microstructure in the sprayed coatings. In general, however, the rapid cooling phenomenon in the plasma process is manifested in extremely fine grains and metastable phases very much akin to those observed in liquid-quenched (LQ) materials. Aspects of the adhesion question have been studied in this program and have been discussed in previous annual report (3-5).

A great deal of study has been dedicated to the microstructures of splat cooled materials. Much work has been carried out on splat cooled ($\sim 10^6$ °C/sec) light metals and alloys, and these studies have in fact been of use to us in understanding the microstructures of thermal sprayed materials, which have their origins in the very rapid solidification rates that they experience.

The higher melting point metals and oxides (>1500 °C) require specially-designed apparatus, and only limited research on their structure and properties has been carried out. However, with the advancement in laser technology and other high energy heating systems, rapid thermal cycling of these materials has become conveniently accomplished. On the other hand, the plasma flame process, because of its extremely high temperature (>6000 °C) can be a more economical method for rapid cooling of both metals and oxides. In addition, the continuous nature of the spraying process can result in a larger quantity of splatted materials which usually cannot be attained with other techniques. Moreover, the post-quench processing (e.g., pressing extrusion) which is usually required in the conventional techniques is eliminated in thermal spraying because in the latter technique, any complicated shape and geometry may be sprayed.

The scope of the present study has been to examine the microstructure of thermal-sprayed coatings in detail and relate that microstructure to their physical properties. An important technological aspect of the sprayed coatings is porosity, which depends, among other things, on particle morphology. This program has included an analysis of porosity, its size distribution, and how these factors can be influenced by the proper selection of coating materials.

Previous reports (3-5) originating from this program have outlined the range of microstructural studies which have been carried out. In the present report for the 1978-79 period we present microstructural considerations on plasma sprayed Al_2O_3, Al_2O_3-TiO_2, and TiO_2 and the attendant phase transformations which occur in these industrially important coatings. Also, presented will be a development on NDE of these coatings using Acoustic Emission.

IV PLASMA-SPRAYED OXIDES

A. Phase Transformations in Alumina Coatings

A detailed x-ray analysis of plasma-sprayed alumina coatings was performed using both Debye-Sherrer photography and powder diffractometry. The crystal structure of the as-sprayed high purity $A\ell_2O_3$-2.5 wt% TiO_2 was found to conform with the cubic metastable phases of alumina rather than with the corundum phase. Similar results were found for sprayed pure alumina. Therefore, greater emphasis was placed on $A\ell_2O_3$-2.5 wt% TiO_2, so that the role of titania additions could be determined.

In general, the as-sprayed alumina coatings were composed of the γ-$A\ell_2O_3$ as the major phase and the δ and θ polymorphs as the minor constituents. The formation of a metastable phase is understandable because the rapid cooling of the molten particles limits the ordering of oxygen and aluminum atoms into the stable α-phase. Positioning of the $A\ell^{3+}$ in the tetrahedral and octahedral groups of oxygen ions determines the final structure of the alumina. Upon slow cooling from melt, the $A\ell^{3+}$ ions, due to their greater mobility than oxygen, can diffuse into the octahedral sites and,thus, reduce the overall free-energy of the system. The resulting structure is the hexagonal α-$A\ell_2O_3$. On the other hand, rapid cooling results in tetrahedral coordination, and the characteristic cubic structure is formed. Moreover, the solidification rate of the particles determines the degree of order and the formation of the intermediate metastable crystal structures. The previous studies of the liquid quenched (6) and vapor deposited alumina (7) have identified γ-$A\ell_2O_3$ as the primary phase (highest cooling rate), while the intermediate polymorphs are basically δ and θ-$A\ell_2O_3$. The transition sequence is generally in the order of γ, δ, θ, into α-$A\ell_2O_3$.

According to these observations, the addition of the 2.5 wt% TiO_2 to the fused alumina powder does not have an apparent effect on the tendency to form non-equilibrium phases in the coatings. A combination of γ and δ-Al_2O_3 phases is present in all of the as-sprayed coatings prepared using ordinary spraying parameters. However, excessive torch heating of the coatings can accentuate the formation of θ and α-Al_2O_3.

Using the integrated intensity of the appropriate x-ray diffraction peaks, an attempt was made to quantitatively determine the volume fraction of each phase in the sprayed coatings. However, a conclusive result was not obtained because of the process-dependence of the spraying and due to the variations of the thermal history of the particles which form the coating. In addition, the crystallographic similarities of the δ and γ-Al_2O_3 make it extremely difficult to quantify the exact volume fraction of each phase within the alumina coatings.

The x-ray analysis can, however, reveal something of the dependence of the coatings structure on the spraying process. For example, since γ-formation is associated with higher cooling rates, the thin alumina coatings (< 200 μm) were found to contain higher fractions of γ-Al_2O_3 and very little θ-phase. On the other hand, thick coatings, where considerable plasma torch heating occurs, are usually composed of the intermediate phases (eg., δ and θ-Al_2O_3). Similar results are obtained with excessive pre-heating of the substrate prior to spraying. Also, coatings sprayed on air-cooled substrates contained larger amounts of δ-Al_2O_3 than those sprayed on water-cooled surfaces.

The size and orientation of the grains in the aluminum metal coatings has been shown in this program to depend on particle morphology and location within the coating (3-5, 8, 9). Similar effects were found with respect to the crystal structure and various phases of the alumina coatings. That is, the cooling rate within each particle governs the structure upon solidifi-

cation, whereas subsequent transformation to the intermediate polymorphs is controlled by the location of the particles and the rate of heat-extraction through the substrate.

1. The Effect of Coating Thickness

To study the effects of coating thickness, a series of x-ray experiments were conducted in which polished surfaces of alumina coatings, at various distances from the substrate, were examined. Substrate-free alumina coatings were sprayed and then mechanically polished to various thicknesses from the top surface. The substrate temperature and, more importantly, the gun-traverse-rate were kept constant in all of these experiments. Using the x-ray diffractometer, and integrated intensity techniques, it was found that the coating-substrate interface contained more γ-$A\ell_2O_3$ than the top (outside) surface of the coating. However, the difference was rather insignificant for coatings up to approximately 450 μm (.0018"). On the other hand, for thicker coatings, the top surface contained considerably less γ-$A\ell_2O_3$ and was predominantly composed of the intermediate δ and some θ-$A\ell_2O_3$ phases. For the very thick coatings (>1700 μm), the top surface contained mostly θ and α aluminas, with very little δ and practically no γ-$A\ell_2O_3$. Furthermore the overall γ-content of these coatings, as determined by the x-ray analysis of the pulverized samples, was usually less than 20% of the total.

For a better understanding of the polymorphism in alumina coatings, TEM and electron diffraction were employed. Although TEM revealed large structural variations within the coatings, the overall result correlates closely with x-ray diffractometry. In regions near to the substrate, the predominant phases were γ and δ-$A\ell_2O_3$, whereas θ and α-$A\ell_2O_3$ (i.e., those phases associated with lower cooling rate) are commonly found at distances away from the interface. Occurrence of both α and the metastable alumina in LQ samples was also reported by Krepski (10) who used TEM to examine

the hammer-and-anvil quenched laser-melted rods.

In general, TEM revealed some mottling within the grains which suggests partial phase decomposition in the as-sprayed alumina coatings. Phase transformation can be further examined by subsequent heat treatment of the sprayed coatings. For example, specimens were heated *in situ* within the microscope revealing sub-structures within the grains. The corresponding SAD pattern indicates the formation of γ-$A\ell_2O_3$ which, according to Lippens and deBoor (11), is the ordered cubic γ-phase and is composed of three sub-cells of spinel-like structure.

2. Role of Particle Size on the Structure of Sprayed Alumina Coatings

The presence of the various phases of alumina in the sprayed coatings does not depend on solidification alone. Thermal history of the particles prior to impact will also be determining as to what phases form. Of particular importance is the particle size, since this controls the extent of particle heating by the plasma flame through boundary-layer conduction. To examine the role of this parameter, a series of x-ray experiments were carried out. In these experiments the size of particles was closely controlled.

The as-received powder of $A\ell_2O_3$-2.5 wt% TiO_2 was dried and then sprayed into water. The quenched particles were then collected, rinsed with methanol, and dried. Most of the particles were spherical, indicating complete melting, although some unmelted angular particles were also present. The spherical particles were separated from the unmelted by a segregation technique using a polished aluminum plate. The collected powder was then screened to several size fractions by a sonic sifter in the following size ranges: < 20, 20-37, 3744, 44-53, 53-62, 62-74, 74-88, all in μm. The coarser powders were ball milled to < 37 μm to eliminate grain size effects in the x-ray powder study.

The results of these experiments are summarized in Fig. (1), where the volume fraction for the α-phase is plotted against the average particle diameter. It is observed that α-$A\ell_2O_3$ is practically absent in particles up to 20 μm in diameter. Traces of α-alumina which were found in these small powders probably originated from the unmelted fine particles which were collected from the water chamber. Combined optical microscopy and Debye-Sherrer x-ray studies indicated that all of the spheroidized particles with $d \lesssim 20$ μm were composed of metastable aluminas. Furthermore, γ-$A\ell_2O_3$ constituted the major fraction of the powder although some δ-phase was also present.

The α-alumina formation is enhanced as the diameter of the particles increases, to the extent that particles of 44-53 μm in diameter contain about 50% α-$A\ell_2O_3$ when quenched into water. The metastable phases of alumina were never found in particles larger than 93 μm. Such a phenomenon is indicative of the effect of cooling rate on the polymorphic structure of alumina within the solidified particles. The fastest cooling occurs in the smaller particles and results in γ-$A\ell_2O_3$, while in the larger particles cooling rates are sufficiently low so that $A\ell^{3+}$ ions can diffuse to form the ordered α-$A\ell_2O_3$ structure.

When the alumina particles are sprayed onto highly conductive surfaces, as in the case of sprayed coatings, higher solidification rates are expected. The fact that the major phases comprising the sprayed coatings are metastable does indeed suggest that solidification rate in the flattened droplet is higher than that for spherical particles. However, the role of the particle size on crystallographic structure of the coatings will be, in general, similar to that observed in water-quenched experiments. That is, the fraction of retained stable α phase will be still higher in the larger flattened particles although to a lesser extent than that shown in Fig. (1).

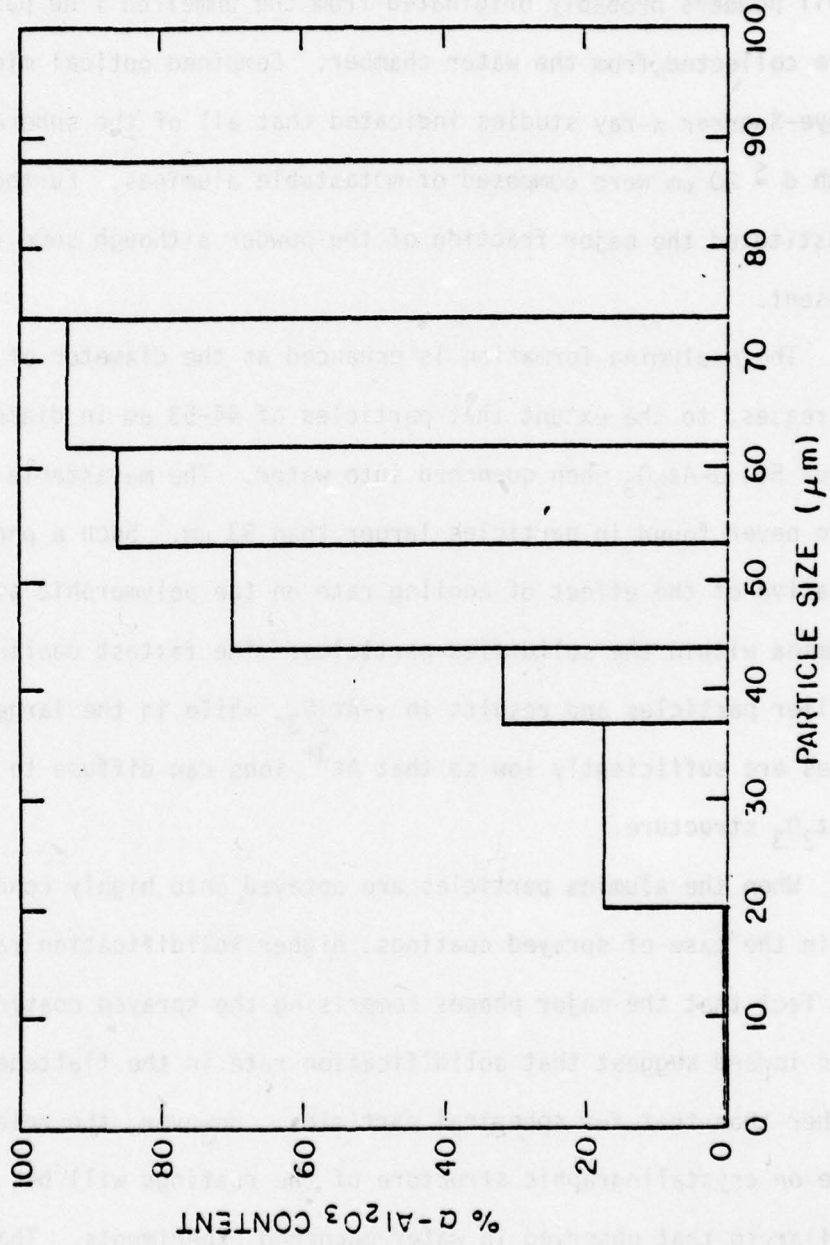

Fig. 1 Particle size vs. % α-Al_2O_3 content in alumina particles sprayed into water.

Another difference between the water-quenched particles and the sprayed coatings which should be considered is the role of fine particles. Since all of the very fine particles cannot be collected from the water, or are lost during the screening, the volume fraction of the metastable phase is certainly higher than what is presented in Fig. (1). The presence of these fine particles and the thermally conductive metal substrate can explain the formation of γ and δ aluminas as the major phases in the sprayed alumina coatings.

B. Structure of Al_2O_3-TiO_2 Coatings

1. Al_2O_3-TiO_2 Solid Solutions

The addition of titanium dioxide to alumina results in a considerable enhancement in the structure of the sprayed coatings. These coatings are observed to have higher cohesive bonding and, thus, porosity was drastically reduced in comparison with pure alumina (12). The enhanced sintering of the TiO_2-containing alumina droplets is generally in agreement with Bagley's sintering study of Al_2O_3-TiO_2 system (13). It is found that additions of up to 0.13 wt% TiO_2 can increase the intrinsic diffusion coefficient of alumina by a factor in excess of 100.

Furthermore, rapidly quenched pure alumina and Al_2O_3-2.5 wt% TiO_2 were found, within the experimental limitations, to possess identical metastable phases. The addition of the TiO_2 phase apparently does not effect the formation kinetics of any of the several polymorphs. The important question arising from this observation is the solubility of Ti ions in the metastable aluminas. The equilibrium solubility of titanium oxide in α-Al_2O_3 is limited to about 0.4 wt% in air (14), and 2.0 wt% in a hydrogen environment (15). The solid solution limits of titanium oxides in the metastable alumina are, however, not well known.

To determine the nature of titanium oxide and its solubility in the sprayed alumina coatings, the fused powders, containing 2.5 and 15 wt% TiO_2, were selected since they were found to be more homogenous than the other compositions tested. Lattice parameter measurements were made according to the method of McKee and Aleshin (15) by using the measured shifts in selected diffraction peaks and comparing these with pure alumina. However, the solubility limit of TiO_2 in sprayed alumina, calculated from the change in unit-cell dimensions, varied greatly for the different samples and compositions. Therefore, the solid solution of TiO_2 could not be represented by a single value; in the coatings containing 2.5 wt% TiO_2, the limit varied from 0.45 wt% to approximately 2.5 wt%, while for the Al_2O_3-15 wt% TiO_2 fused powder, the coatings showed solubility limits as high as 4.35 wt% TiO_2.

The variations in the solubility limits can possibly be explanined by the phenomena taking place during the spraying process: the particles which are introduced into the plasma flame are heated to temperatures close to as well as above their melting point, followed by rapid cooling and further torch heating. Analysis of the coatings composed of an aggregate of such particles will only reveal a spectrum of solid solutions of titanium oxide in the alumina rather than a specific phase. However, Gani and McPherson (16) found solid solutions in δ-Al_2O_3 to at least 15 wt% TiO_2 in the fine particles prepared by high frequency plasma oxidation of $TiCl_4$-Al_2Br_6 mixtures. For the compositions containing 28.4 to 56.9 wt% TiO_2, the condensed particles were found to be composed of rutile precipitates in δ-Al_2O_3. It is, therefore, conceivable that plasma-sprayed alumina coatings may permit higher solid solutions of titanium oxide than found in α-Al_2O_3. In fact, it is likely a non-stoichiometric titania in the sprayed powder which gives rise to enhanced solubility in alumina. The reducing environment of the plasma results in some reduction of the titania

and, therefore, the higher values obtained for Al_2O_3-15 wt% TiO_2 correspond mainly to the solubility of suboxides of titania.

2. Phase Separation in Al_2O_3-TiO_2 Coatings

The physical properties (e.g., density, hardness) of the coatings formed from the composite and fused powders containing more than 2.5 wt% TiO_2 are very similar, whereas the microstructures are considerably different. The Al_2O_3-13 wt% TiO_2 composite powder results in coatings with excessive free alumina and limited aluminum titanate compound, as indicated by x-ray analysis. TEM studies of these coatings revealed limited areas in which the two oxides had reacted. The Al_2O_3-40 wt% TiO_2 composite powder, however, undergoes extensive alloying upon spraying, and the microstructure of these coatings were very much akin to those of fused powders.

The as-received fused powders were homogeneous mixtures of α-Al_2O_3 and β-Al_2TiO_5. Upon spraying, the phase distribution changes, and the final composition of the coating depends on the extent of phase decomposition during the deposition of the molten particles. In general, because of rapid solidification, partial phase decomposition is observed in the coatings, although post-spray annealing or extensive torch heating can also result in phase separation within the alloyed oxide coatings. Substrate-free coatings of Al_2O_3-15 wt% TiO_2 were sprayed and prepared for TEM study. A non-homogeneous phase separation is usually evident in the mottled grains throughout the sprayed coatings. Later annealing of these coatings caused further decomposition of the supersaturated matrix. Figure (2) shows a TEM micrograph and the corresponding SAD pattern of an area within a coating which was annealed in air at 500°C for one hour. Precipitation has occurred both at the grain boundaries and in the grains, although in the latter case, the plate-like precipitates seem to be preferentially oriented along two orthogonal directions. The x-ray analysis

indicates that these coatings contained mostly δ and γ-Al_2O_3, with some intermediate β-Al_2TiO_5 compound.

Unlike metal coatings, alumina and other pure oxide coatings examined by TEM do not generally contain lattice defects such as dislocations or vacancy loops. However, an interesting observation during the study of alloy oxide coatings has been the occurrence of dislocation networks in the sprayed coatings containing about 40 wt% TiO_2. Figure (3) presents the TEM micrographs of two types of dislocations found in Al_2O_3-40 wt% and 41 wt% TiO_2 composite and fused, respectively, coatings. For the composite coatings, dislocations have been observed in the form of resolvable networks, interacting with inclusions and voids within the grains, as shown in Fig. (3a-b). On the other hand, the fused coatings contained arrays of dislocations similar to low-angle subgrain boundaries (Fig. 3c).

Although rapid solidification from the melt is responsible for the occurrence of lattice defects, experimental study pertaining to such phenomena in Al_2O_3-TiO_2 alloys could not be found. Recently, Tkachenko, et al. (17) in an investigation of the wear resistance of Al_2O_3-40 wt% TiO_2 detonation-formed coatings, have reported the presence of the Ti_9Al_{23} intermetallic compound. The coatings also contained α-Al_2O_3 rather than the usual metastable cubic forms. It has been suggested that the intermetallic compound reduces the brittleness of the oxide matrix and, thus, contributes to the enhanced surface wear characteristics of these coatings.

X-ray diffractometry indicated the aluminum titanate (β-Al_2TiO_5) to be the major phase in the Al_2O_3-40 wt% TiO_2 coatings. The coatings sprayed with the composite powder contain minor amounts of alumina solid solution. The aluminum titanate which is formed when the solubility limit of TiO_2 is exceeded has a pseudo-brooksite orthorhombic crystal structure, similar to Fe_2TiO_5 and melts congruently at 1860°C (18). The x-ray results for Al_2O_3-TiO_2

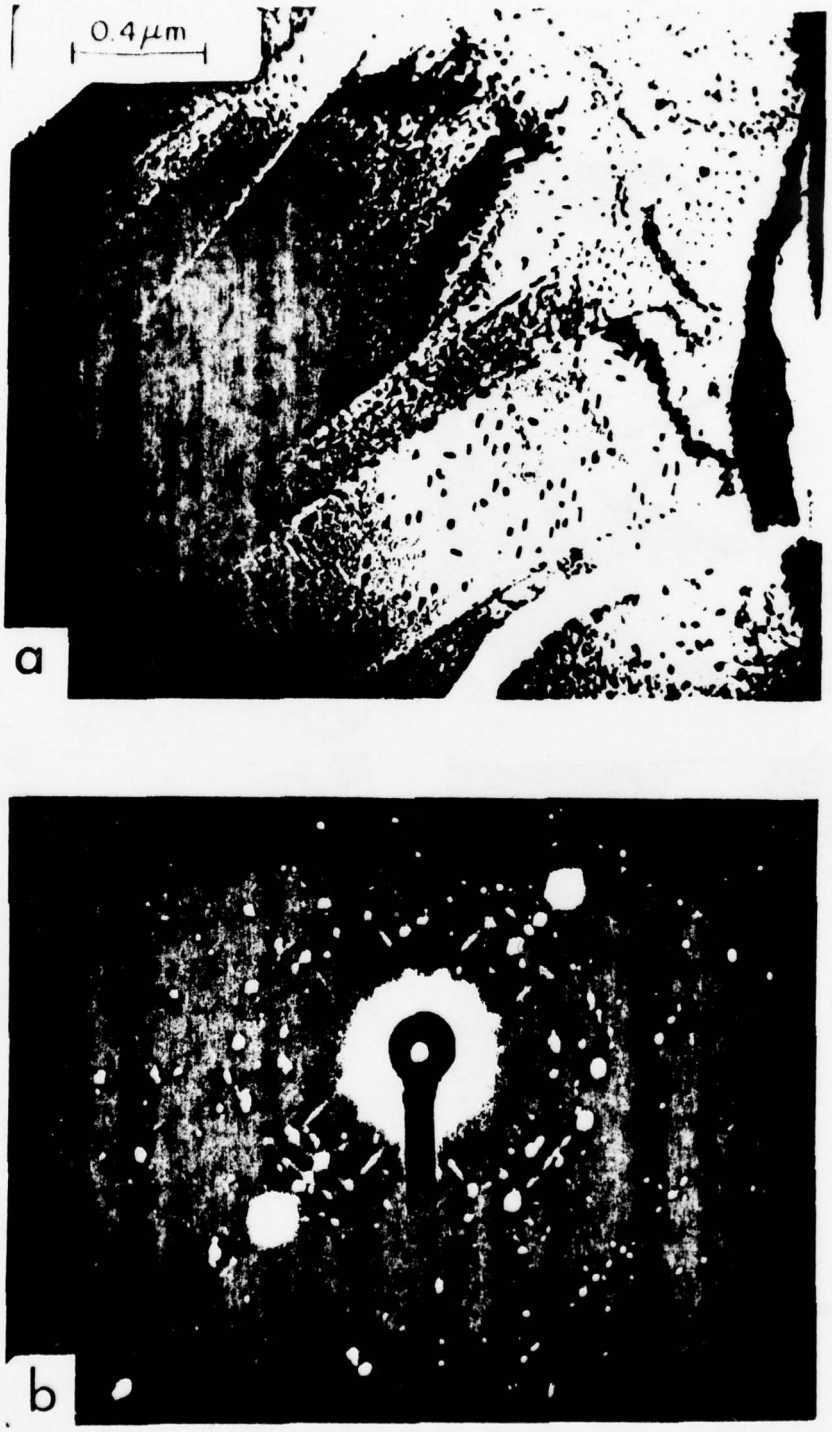

Fig. 2 TEM micrograph of annealed (500°C) Al_2O_3-15 wt% TiO_2 coating showing the precipitates (a), and the corresponding SAD pattern (b).

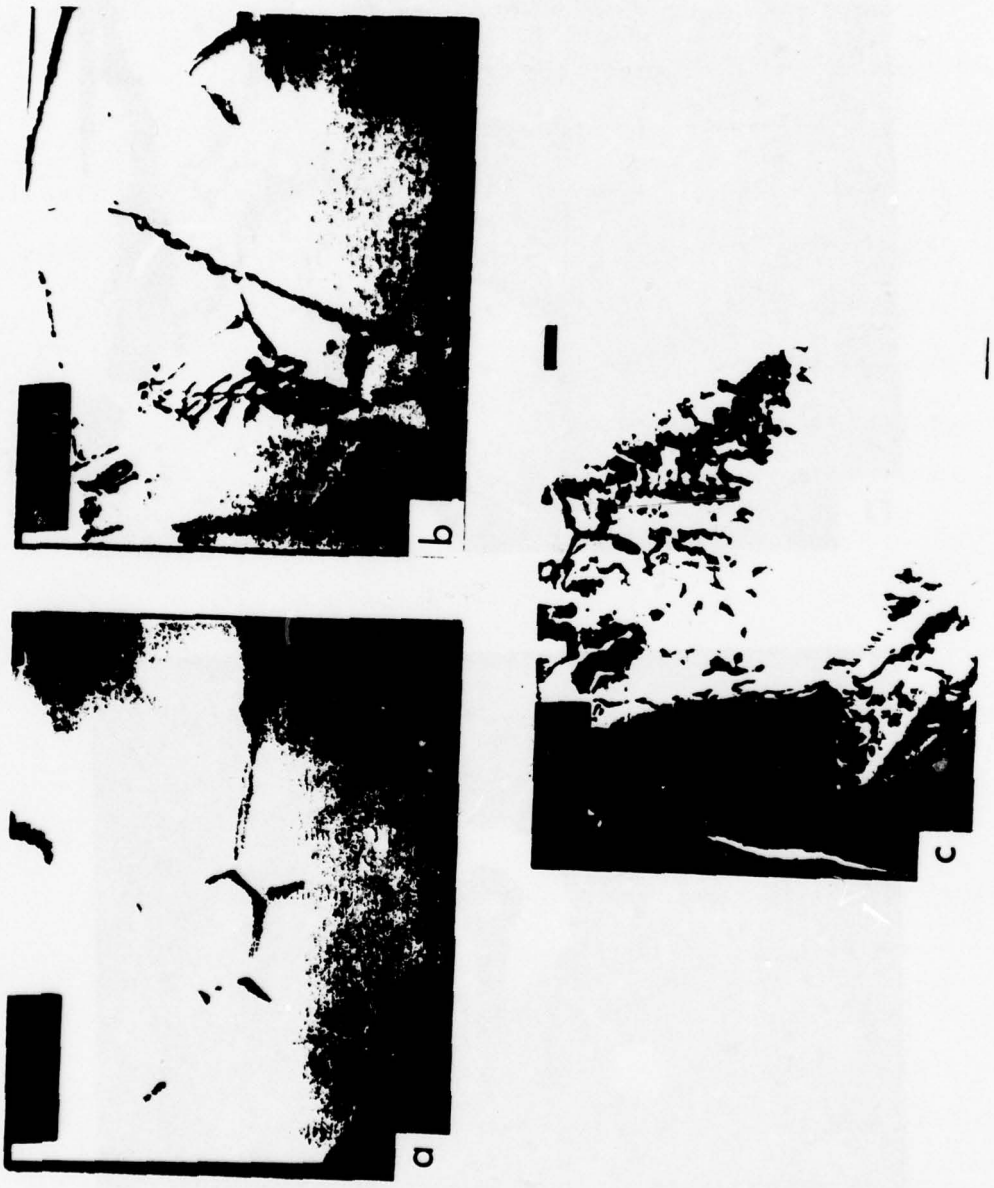

Fig. 3 Dislocation network in plasma sprayed Al_2O_3 40 wt% TiO_2 composite coatings (a, 43200X; and b, 53700X). Defects observed in Al_2O_3 41 wt% TiO_2 fused coatings (c, 45000X)

coatings indicated only the low temperature β-Al_2TiO_5, which is stable to 1200°C, and below which decomposes by a eutectic reaction to Al_2O_3 and TiO_2. The high temperature α-form was not detected, however this phase is said to transform readily into the β-Al_2TiO_5 upon cooling, especially in the presence of impurities such as Fe_2O_3 (18).

The formation of aluminum titanate similar to $MgAl_2O_4$ spinel formation is accompanied by a volume expansion of ∿ 10% (19). In addition, although titanium dioxide has no intrinsic effect on the strength of alumina when in solid solution, it decreases the fracture strength when present as titanium-dioxide-rich, or titanate second-phase (20).

The fact that most of Al_2O_3-TiO_2 alloy coatings are composites of several phases, large residual stresses usually result within the coatings due to the thermal expansion mismatch. Such internal stresses place a thickness limitation on these coatings and can cause delamination. More significantly, since the titanate phase which may form by the reaction of Al_2O_3 and TiO_2 oxides, has very poor mechanical strength (19), it fractures easily under the influence of the stress. The preferential microcracking of the titanate phase has been observed in this program in Al_2O_3-13 wt% TiO_2 composite coatings at the particle boundaries. The microcracking phenomenon is, perhaps, responsible for the enhanced wear resistance of the Al_2O_3-TiO_2 coatings. A similar mechanism is found to cause the strengthening of partially stabilized zirconia (PSZ) in which the transformation-induced microcracks prevent fracture by arresting the crack propagation (21).

3. Noncrystalline Phases in Al_2O_3-TiO_2

The rapid solidification of the oxide particles has been shown to result in lattice defects and extension of the solid solubility limit in the Al_2O_3-TiO_2 system. Another feature of the very high solidification rates is the formation of a noncrystalline solid (NCS) constituent in

Al_2O_3-40 wt% TiO_2. However, the metastable glassy phase was found only in the particles rapidly solidified from the melt on high-conductivity metal surfaces.

The composite and fused alumina powders containing approximately 40 wt% TiO_2 were plasma sprayed on water-cooled polished substrates. A very high solidification rate from liquid is assured by moving the plasma torch rapidly over the substrate. In fact, the splatted particles which adhere to the polished surface are truly liquid quenched since the unmelted or partially solidified-particles do not adhere to the surface. The particles were examined under TEM directly or after ion-thinning. The NCS phase was only observed in the thin region on the edges of the splatted particles where the solidification rate is higher. The presence of a glassy phase was noted by the diffuse SAD pattern. Other regions, within the particles, showed the fine, crystalline structure which is usually found in the sprayed oxides.

In order to further examine the glassy structure, the NCS areas were heated in situ in the electron microscope and the crystallization was examined. Figure (4) shows the TEM micrograph of NCS phase which was crystallized under the electron beam. The diffuse SAD pattern before and after crystallization is shown in Fig. (4b) and Fig. (4c) respectively. The formation of the fine crystalline phase within the glass phase occurred very rapidly on heating. The crystallization usually began at the edges of the thin foil, which is heated more rapidly, and propagated toward the interior of the foil. However, some areas showed rapid crystallization (almost explosively) throughout the sample.

Glass formation theories in ionically-bonded materials and, in particular, the NCS phases have been the subject of many investigations. According to current concepts, the binary system Al_2O_3-TiO_2 cannot form a glass under equilibrium conditions and even upon rapid solidification

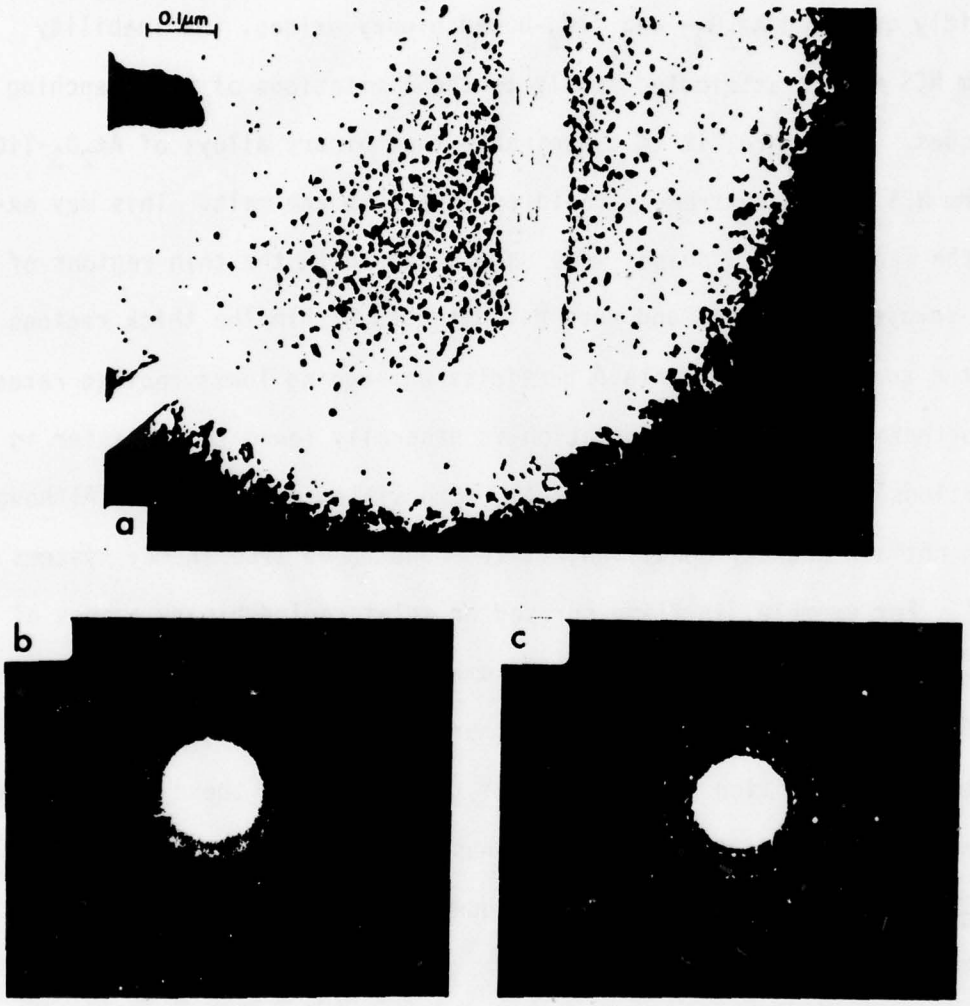

Fig. 4 TEM micrographs of plasma sprayed Al_2O_3-41 wt% TiO_2. Crystallized region (a); SAD patterns before and after crystallization (b and c).

from melt. However, glass phases are found in some restricted ranges of complex compositions. Therefore, the observation of a NCS phase in sprayed Al_2O_3-40 wt% TiO_2 cannot be explained in light of any of these concepts. Suzuki and Anthony (22) have also found a crystalline structure in rapidly quenched Al_2O_3-TiO_2 oxide containing 20 mol% Al_2O_3. However, as suggested by Takamori and Roy (23) who examined the NCS phase formation in a number of rapidly quenched Al_2O_3- and TiO_2-based binary oxides, the inability to form NCS may be attributed simply to the limitations of the quenching techniques. Therefore, it is conceivable that binary alloys of Al_2O_3-TiO_2 may form NCS through extremely rapid cooling from the melt. This may explain the fact that NCS phases were only observed in the thin regions of the as-sprayed particles, and were not detected within the thick regions or in the coatings which contain particles undergoing lower cooling rates.

Furthermore, the glass formation is generally found to be easier in compositions close to the deep eutectic composition of a system. Although this is not a necessary condition, it is found to be true in may systems (23,24). For example, in flame sprayed or splat cooled binary oxides of Al_2O_3-SiO_2, Al_2O_3-Y_2O_3, TiO_2-BaO, and some others, the highest crystallization temperature and stability regions are found to be associated with the eutectic composition of each systems (23). Based on these observations and the examination of the Al_2O_3-TiO_2 phase diagram, it may be suggested that NCS phases can be formed by rapid quenching from liquid for compositions containing about 40 wt% TiO_2.

C. Microstructure of Sprayed Titania Coatings

Although stoichiometric titania possesses a well characterized tetragonal symmetry, it can lose oxygen readily and form a number of closely related suboxides (Magneli phases). The nature of slightly reduced titanium dioxide has long been the subject of many comprehensive investigations. However, very little is said about the structure of rapidly-quenched titania,

and the formation of non-stoichiometric suboxides.

The as-received powder was mainly composed of rutile, although lattice parameter measurement showed traces of slightly reduced oxide, which is commonly found in such fine titania powders. Upon spraying, however, this oxide undergoes extensive reduction and the change in oxidation state of Ti ions is accompanied by a color change from yellowish-white to a blue-black. In addition to rutile, a reagent grade anatase powder was also obtained and sprayed under similar conditions. The sprayed coatings thus-obtained had a rutile crystal structure, and were in general identical to those prepared by the previous powder. Furthermore, both types of coatings were extremely temperature sensitive and showed local discoloration because of overheating during the spraying process.

Substrate-free titania coatings were plasma sprayed to approximately 750 μm thickness and then ball milled to -400 mesh (< 44 μm) size for x-ray analysis. The coatings were found to consist of the oxygen-deficient rutile and the Magneli phases ($Ti_n O_{2n-1}$, $4 \leq n \leq 10$). Following the Ti-O phase diagram and the x-ray study of Anderson et al. (25) the various phases present within the sprayed coatings were identified. In the coating sprayed with a Ar/H_2 plasma in air, the phase with the highest degree of reduction from stoichiometric TiO_2 which could positively be identified was Ti_4O_7. Concurrently however, were a number of other phases closely related to the reported structures (25) of Ti_5O_9, Ti_8O_{15}, Ti_9O_{17}, and $Ti_{10}O_{19}$. All of the above oxides of titanium have a triclinic structure with nearly equal unit cells. Therefore, quantitative determination of each phase was difficult, particularly since some spray-technique dependence was observed for the various phases present in the coatings.

The formation of an oxygen deficient lattice in rutile is accommodated by the production of structural defects. For the sprayed titania, the defects are mostly formed in the particles at high temperature near the melting point (1830°C) and are retained in the rapidly solidified layers. At room temperature, the defects are normally found to be in the form of planar crystallographic shear (CS) planes. A TEM micrograph of an ion thinned rutile coating clearly reveals the planar faults found in parallel bands throughout the polycrystalline region (Fig. 5). The transgranular and intergranular cracks are caused by the thinning process during the sample preparation. Electron diffraction analysis of similar areas within the various samples indicated that the shear planes were mostly parallel to one of the {132}, {101}, or {121} planes of the rutile structure. Bursill et al. (26) have suggested an ordering mechanism operating within the reduced rutile matrix which is dependent on the concentration and the type of defects. According to their results, the disordered {132} and {101} planar defects form in the TiO_{2-x} ($x \sim 0.005$) phases, and as the defect concentration is increased ($0.1 \leq x \leq 0.25$), the orientation of the defects is ordered into {121} shear planes. The presence of all these shear planes in the sprayed titania, as observed by TEM, indicates that the rapidly solidified layers are composed of a mixture of the Magneli phases of rutile, which is consistant with the x-ray results.

The ordering phenomenon of the defects in nonstoichiometric rutile is also found in the present TEM study. Since the rapid cooling rates achieved in plasma spraying can practically freeze-in the high-temperature microstructure, the early stages of ordering of defects in reduced rutile could be examined. Thin layers of rutile were sprayed onto a water-cooled metal surface by rapidly traversing the plasma gun. TEM examination

Fig. 5 TEM micrograph of plasma sprayed TiO_2 containing elongated defects (a) and SAD pattern (b). The defects are caused by the oxygen loss during spraying.

of the ion thinned samples revealed a defect morphology different from those shown earlier. Figure (6) presents bright and dark-field images, and the corresponding SAD pattern of an area which contains a large number of singul and network dislocations. There is a high concentration of dislocation loops, some forming a network of low-angle grain-boundary-type morphology. It is believed that the dislocation loops can interact with the oxygen vacancy clusters which form on the {132} planes during the early stages at low oxygen vacancy concentrations (27). The shear planes grow by trapping more vacancies and form needle-like defects on the {132} planes in the rutile. In the areas within the sprayed rutile, with greater reduction from stoichiometry, the {132} shear planes are eventually ordered into {121} planes. However, the exact mechanism for the latter process is not well understood.

The degree of reduction from TiO_2 composition is of considerable importance since it might well influence the properties of the sprayed coatings. For example, the dense structure of the pure titania coatings, or the densification observed in Al_2O_3-TiO_2 mixed coatings as influenced by TiO_2 content, may be due to the presence of non-stoichiometric rutile phases. The suboxides of titania melt at temperatures considerably below stoichiometry TiO_2. Also, because of their oxygen-deficient structure, these suboxide grains can wet other oxides (e.g., Al_2O_3) more readily and, therefore, increase the particle-particle cohesive strength. On the other hand,structural defects and non-stoichiometry can effect the strength of the oxide structure. For slightly reduced polycrystalline titania this effect was shown by a larger than 30% decrease in elastic modulus for only a 2% change in stoichiometry (28). Therefore, strengthening of the TiO_2-containing coatings, due to improved particle bonding, is impaired by the lower strength of the free titania grains.

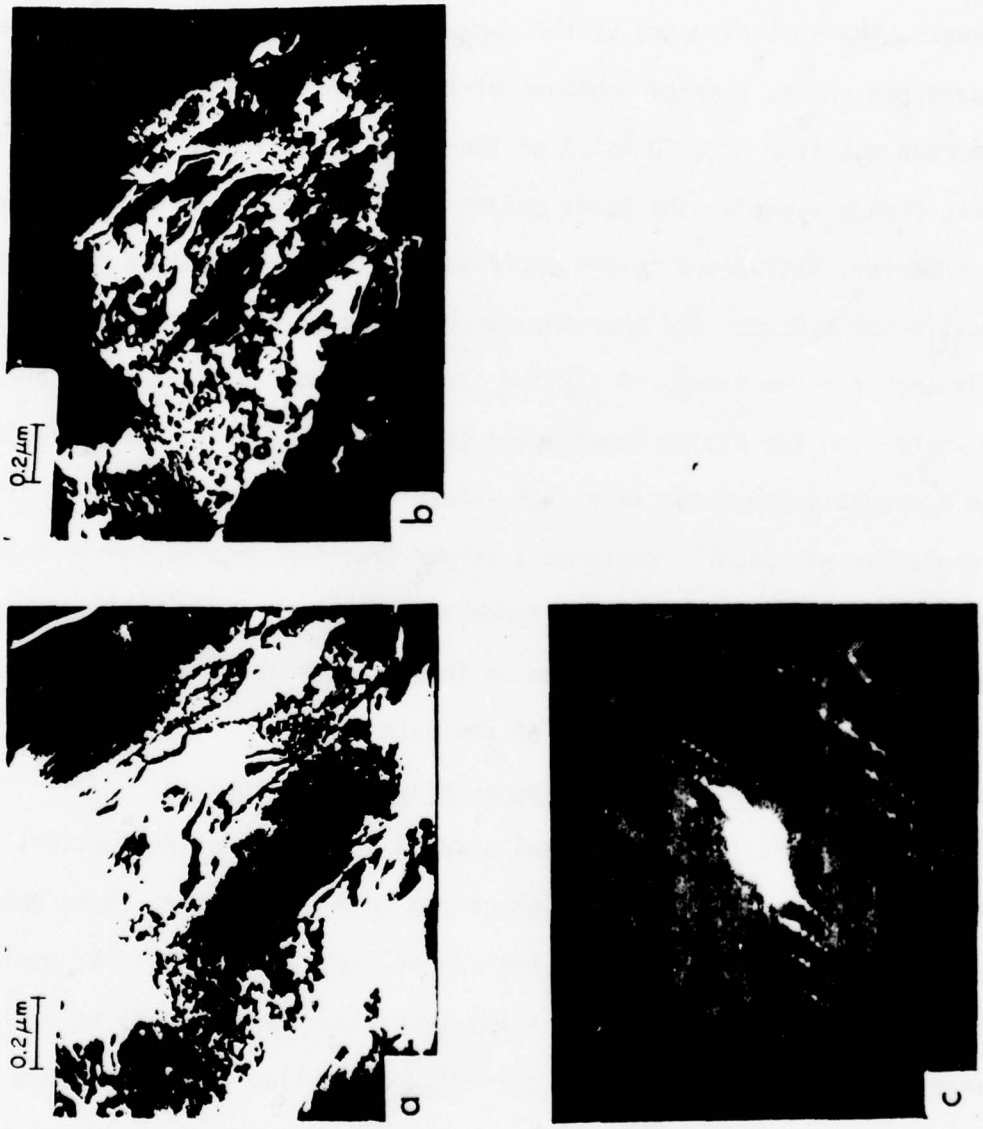

Fig. 6 TEM micrographs of sprayed TiO_2: BF, DF, and the corresponding SAD pattern a-c, respectively

As mentioned earlier, the lowest composition of titanium oxide observed here in the sprayed coatings was that of Ti_4O_7. The oxides with lower oxygen content are Ti_3O_5 and Ti_2O_3, which possess monoclinic cell structure and have a limited range of homogeneity. Neither of these oxides were detected in the coatings sprayed with Ar/H_2 plasma in air. However, the stoichiometry of the sprayed titania coatings showed some dependence on the hydrogen content of the plasma; changing the secondary hydrogen gas from 5 to 20 vol.% of the argon primary resulted in a slight phase change towards the lower oxides (e.g., Ti_4O_7). This phenomenon is, however, attributed to the increase in plasma temperature due to the addition of hydrogen and thus the superheating of the rutile particles injected into the flame. A similar trend in oxygen dificiency is obtained by increasing the plasma temperature (via increased KVA), while keeping the hydrogen content the same. It should be added that the plasma flame operated in air usually contains a larger fraction of atmospheric oxygen which can oppose the effects of hydrogen addition. It is believed that the spraying of titania in vacuum or inert controlled chambers might result in a substantial reduction of the oxide.

D. Acoustic Emission Study of Plasma-Sprayed Oxide Coatings

A major deficiency of thermal sprayed protective oxide coatings is their porosity. This porosity, which can lead to fracture, comes about from the thermal spray process, but can be largely controlled by modifying powder particle size as well as spray velocity. The porosity normally ranges from several percent for carefully controlled plasma spraying to 15 percent for oxyacetylene flame spraying, by volume. Porosity of thermal-sprayed Al_2O_3 can be considerably reduced by oxide additions (eg., TiO_2, ZrO_2,Y_2O_3) (8).

The main concern arising from porosity in oxides is their giving rise to failure by acting as crack initiators. Also, pores might represent paths for easy crack propagation.

As part of this program we sought to use the technique of acoustic emission (AE) to monitor acoustic-generating processes in porous thermal-sprayed oxide ceramic coatings on steel substrates. This AE study is being carried out jointly with Professor K. Ono of UCLA, also a ONR contractee. Non-destructive evaluation (NDE) techniques for such coatings, of the order of 0.005 inches (0.13 mm) thick, are virtually non-existent. We thus employed AE to examine cracking and mechanically-induced pore closure processes in these coatings. It soon became clear that the coating undergoes local densification and/or crack-distribution modification under indentation loading. An initial report of this study is presented here in the hope of stimulating the use of AE techniques for the characterization of oxide coatings for NDE purposes. Though the tests carried out here are not non-destructive, the AE associated with these tests does suggest that strictly NDE tests could in fact be formulated using the AE concept.

A range of aluminas and alumina-titanias have been flame or plasma sprayed in air. The plasma-sprayed oxide coatings were deposited by a 40 KVA non-transferred, dc plasma gun. The flame-sprayed coatings were prepared by a conventional oxyacetylene gun which is modified for the spraying of oxide powders. The spraying parameters were those suggested by the manufacturer and were further optimized for each of the oxide powders.

The cold-rolled mild steel substrates were cleaned and then grit blasted (750 μm angular Al_2O_3 grits) prior to coating. For indentation tests, the as-sprayed coatings (∿25 mils, 635 nm) were ground with 150 nm diamond wheel to a thickness of approximately 23 mils (580 nm). Porosity

was measured by Mercury Intrusion Porosimetry, as described in previous reports and publications (9,29).

For AE measurements, a piezoelectric AE transducer (Model AC 175L, Acoustic Emission Technology Corp. (AETC), Sacramento, CA.) was coupled to the coated sample via viscous resin (Model SC-4, AETC). AE signals were fed to a signal processor (Model 204, AETC) through a preamplifier. Total gain of the system was 94 dB with the threshold level of 1 volt.

The indentation was made at room temperature by a Brinell Hardness Indentor, applied into the coating with a load of 500 kg. The total number of acoustic emission events were recorded digitally on the signal processor during and immediately after the removal of the indentor. Each AE count represents the average of at least six AE determinations.

Table I shows the results for a total of 5 experiments. Note first the difference in acoustic events between plasma- and flame-sprayed alumina. The plasma-sprayed coating had 8 to 9% porosity, and it yielded an average AE counts of about one-half that for the flame-sprayed coating which had about 15% porosity. Additions of titania to alumina reduced the porosity, as well as the observed AE counts. The plasma-sprayed mixed (fused) oxide produced decreasing AE counts with an increase in additive: 40% TiO_2 addition to Al_2O_3 reduces through-porosity by one-half, and also reduces the average number of AE counts by a ractor of about 5. A difference in AE counts between composite and fused powders for 40% TiO_2 additions was not highly significant (however, see below). Note that there was no indication of debonding at the interface after the indentation was made.

The dramatic decrease in AE generation with increase in density suggests that the observed AE phenomena in the oxide coatings studied here are pore-controlled. We have observed from scanning electron microscopy (SEM) that large cracks propagate from the region of the hardness

TABLE I

AE Events (500 kg Load with 10 mm Indentor)

Samples	Porosity (Vol. %)	Total Counts ($X 10^3$)
Al_2O_3 (Oxyacetylene)	15	308
Al_2O_3 (Plasma)	8-9	139
Al_2O_3-13 w/o TiO_2 (Plasma-Fused)	6	85
Al_2O_3-40 w/o TiO_2 (Plasma-Fused)	4	39
Al_2O_3-40 w/o TiO_2 (Plasma-Composite)	4	26

indentation. Such cracking is undoubtedly associated with pores within the structure. An additional possible source of AE will be the mechanically-induced closer of pores.

Of further interest is the difference in AE between the fused and composite (mixed and sintered) Al_2O_3-40 w/o TiO_2. The fused product shows 50% more AE than does the composite. On the other hand, both coatings show similar porosities. The technique of mercury intrusion porosimetry shows only surface-connected pores, whereas it appears that AE is sensitive to all the pores present in the coating.

Further AE tests were carried out on plasma sprayed oxide coatings on steel. These additional tests have involved thermalcycling to test the adhesive bond strengths of the coatings and the role played by differential thermal expansion on delamination between coating and substrate. Tested were Al_2O_3; Al_2O_3 with 2, 13, and 40 wt.% TiO_2; TiO_2; and ZrO_2. The coatings were sprayed onto one end of a 10 cm long steel substrate, the other end to which was attached the AE transducer. The coated end was then placed in a furnace at 820°K and the AE was followed during heating and during air-cooling, after removal of the test specimen from the furnace. The experimental arrangement is shown on Fig. 7.

In Table II is given the results of our preliminary tests. T_s is the temperature at which the AE signals were first detected, total N_H was the integrated AE count from T_s to the maximum temperature of the furnace, and Total N_c was the total AE count on cooling from the maximum temperature to 423°K. Fig. 8 shows AE counts vs temperature for the Al_2O_3 and alloy coatings, and Fig. 9 shows the situation for the three oxides tested.

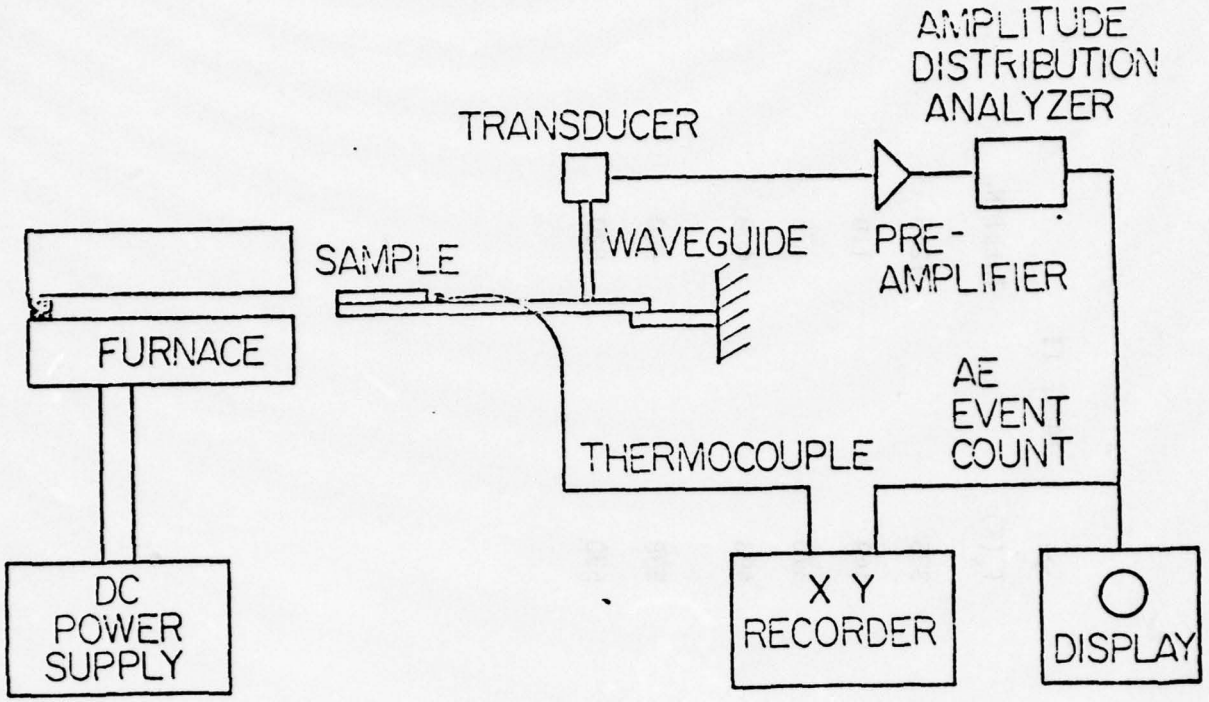
AMPLITUDE
DISTRIBUTION
ANALYZER
TRANSDUCER
WAVEGUIDE
PRE-
AMPLIFIER
SAMPLE
FURNACE
AE
EVENT
COUNT
THERMOCOUPLE
DC
POWER
SUPPLY
X Y
RECORDER
DISPLAY

Figure 7

TABLE II

Sample	T_s(K)	Total N_H	Total N_c
Al_2O_3	396	1265	760
w/2% TiO_2	449	110	80
13% "	570	75	45
40% "	493	408	65
TiO_2	538	380	340
ZrO_2	590	820	180

While this work is currently continuing, initial conclusions can be made. Possible origins of the observed AE signals are microcracking within the oxide coating and adhesion at the coating-substrate interface. Of course differential thermal expansion between coating-and-sbustrate could be the cause of the AE events. Anisotropic thermal expansion between grains may also contribute to microcracking. However, there is apparently no significant effect of AE on coating thickness, which would indicate that the AE was not originating principally within the coating "bulk" itself. (Further studies of the free, self-supported coating will be carried out during the next contract period to resolve this point).

Relative to Table II, it is to be noted that Al_2O_3 is by far the noisiest, with a major decrease in AE resulting from alloying with TiO_2; 13 wt% appears to yield the minimum overall AE counts, with 40 wt% showing an increase in AE. Clearly, the pure TiO_2 and ZrO_2, though lower in overall AE counts than pure Al_2O_3, still show higher AE than does the 13 wt% TiO_2 alloy. This result is consistent with the well known industrial fact that this alloy yields a minimum wear rate.

Thermal expansion measurements of the oxide coatings have begun in an attempt to correlate the above AE results with differential thermal expansion phenomena. The above experiments are continuing.

The details of the sources of AE within oxide coatings must await further experimentation, with particular emphasis on the ultra-microstructure eneath the indentor. Such work is currently underway.

These preliminary measurements indicate that there may be utility in AE as an non-destructive evaluation method for thermal-sprayed coatings.

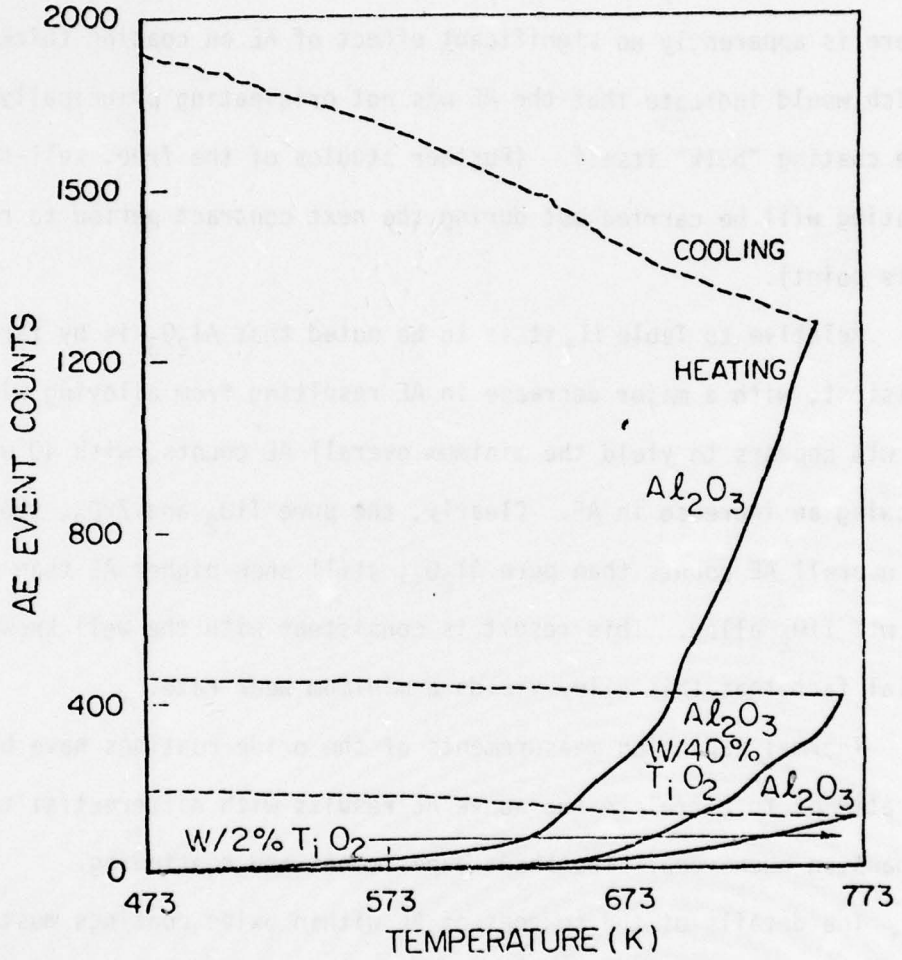
2000
1500
1200
800
400
0
AE EVENT COUNTS
COOLING
HEATING
Al_2O_3
Al_2O_3
W/40% $Ti O_2$
Al_2O_3
W/2% $Ti O_2$
473
573
673
773
TEMPERATURE (K)

Figure 8

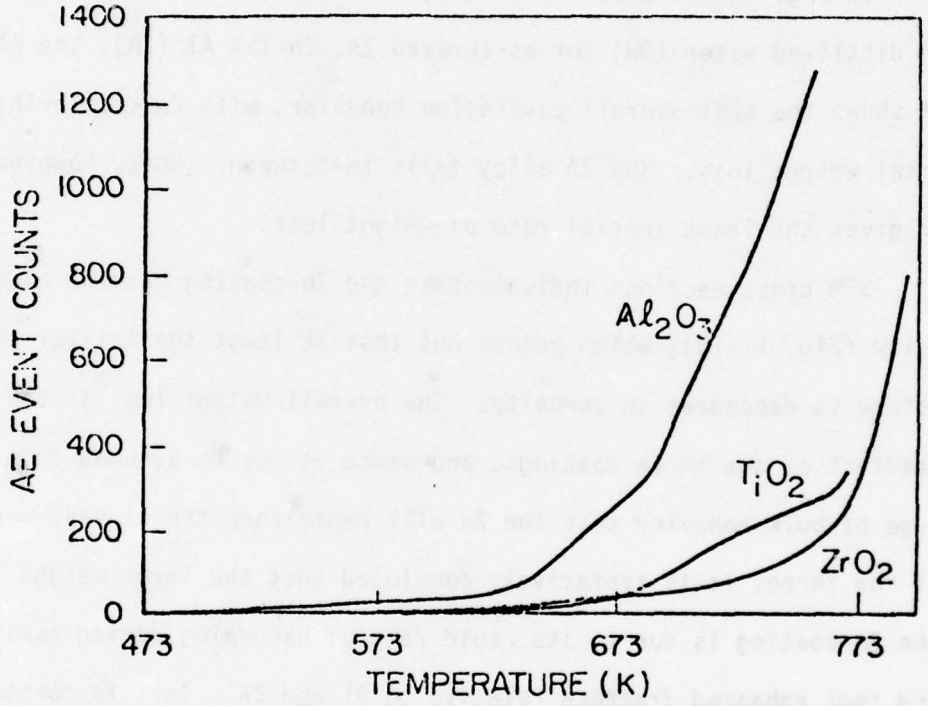
1400
1200
1000
800
600
400
200
0
AE EVENT COUNTS
473
573
673
773
TEMPERATURE (K)
Al_2O_3
Ti_O_2
ZrO_2

Figure 9

Cavitation-Erosion in Distilled Water and in NaCl Solution

In previous reports (3-5) from this program, considerable discussion was presented on both cavitation-erosion and on salt water corrosion. During the last contract period, a synergistic approach was taken relating the mechanical to the corrosive effects. While the main results of this aspect of the program have yet to be developed (the work is currently in-progress), the high points will be reviewed here.

In Fig. 10 are shown three weight loss plots for cavitation-erosion in distilled water (DW) for as-sprayed Zn, Zn-15% Al (ZA), and Al.* Clearly, Al shows the best overall cavitation behavior, with Zn displaying the greatest total weight loss. The ZA alloy falls in-between. Note, however, that Zn gives the least initial rate of weight loss.

SEM cross-sections indicate that the Zn coating has the minimum porosity (Fig. 11-13), which points out that at least the initial cavitation attack is dependent on porosity. The overall weight loss of the Zn is the greatest of the three coatings, and since it may be assumed from our knowledge of bulk behavior that the Zn will experience the highest work hardening of the three, it is tentatively concluded that the large weight loss for the Zn coating is due to its rapid rate of hardening during cavitation, and thus enhanced fracture relative to Al and ZA. This is consistent with cavitation behavior in DW of bulk materials, where Al shows an incubation time prior to weight loss of 45 minutes, and Zn shows essentially none; Figs. 14 and 15.

---

* The materials were all oxyacetylene flame sprayed using the parameters given in Table II. Cavitation was carried out using an exponential horn with WC tip spaced 0.008 inches away from the specimen at a frequency of 20 KHZ. The tip amplitude was 10 μm.

TABLE II

Flame Spraying Parameter*

Coating Metal	Spray Rate	Wire Size	Oxygen			Acetylene			Air		Spraying Distance
			Pressure	Flow		Pressure	Flow		Pressure	Flow	
	(lbs/hr	(in)	(PSI)	(gF)	(ScFH)	(PSI)	(gF)	(ScFH)	(PSI)	(gF)	(in)
Al	12	1/8"	30	44	90	15	40	65	65	53	6"
Zn	32	1/8"	28	45	95	15	42	45	65	53	6"
Zn-15Al	32	1/8"	28	45	95	15	42	45	65	53	6"

*Note: Metco IOE Gun with EC Air Cap was used

On the basis of the above arguement, the ZA alloy would fall in-between the weight loss curves for the two base metals, and, indeed, based on preliminary measurements of bulk ZA, it does.

It is concluded from the above, that pores in themselves are not the main reasons for failure in DW under cavitation attack. However, it is important to note that different behavior is observed in NaCl solution (SW), as will be discussed below.

The rate of weight loss for these coatings is given in Fig. 16 for both DW and SW, as well as for the coatings that have been cold rolled (40% reduction of the coating thickness). The main observation is that the rate of weight loss for the ZA alloy is essentially unchanged, whereas the cavitation-erosion effects for both Zn and Al coatings will very much depend on the liquid.

Potentiometric measurements were coordinated with weight loss measurements using the experimental arrangement shown in Fig. 17. In these experiments, potential measurements were carried out on the cavitation specimen using an interruption technique with the test solution maintained at 25°C. Potential measurements were made at specified intervals, and are plotted together with weight loss for the Al coating in Fig. 18. It is to be noted that the as-flame sprayed coating shows the greatest electrochemical activity, a major shift in potential occurring after 200 seconds of cavitation. The rolled coating is seen to be considerably less active, with the rolled-and-sintered coating showing the least active behavior. As opposed to the weight loss behavior in DW, it is clear that porosity is here playing a key role, since it is well known that both rolling and sintering will substantially decrease porosity: (See Figs. 19 and 20).

In summary, for cavitation in DW, two important effects appear to predominate: pores and work-hardening. The Zn coating, though by far the least porous, shows the greatest overall weight loss in a cavitation field. This, we suggest, is due to the high work hardening rate experienced by the Zn, and is consistent with the results found for bulk material. On the other hand, when the porosity of Al is reduced by rolling, or rolling-and-sintering, the rate of weight loss is somewhat diminished, but this effect we attribute to a decreased porosity. In the case of the ZA alloy coating, when the porosity is found to be slightly greater than for the Zn, work hardening is expected to play a major role in coating degradation.

Conditions of salt water (SW) cavitation-erosion are somewhat different and will be treated separately here. Fig. 16 showed comparisons between DW and SW for the base metals and the alloy in both as-sprayed and rolled conditions. Again, the rate of weight loss for the ZA alloy does not depend on the solution or coating condition. On the other hand, the degradation of the Al coating will depend greatly on the solution, the maximum rate of weight loss increasing from 65 to 80 μgs/sec in DW and SW, respectively.

Cavitation erosion is generally considered to have a mechanical and corrosion component (30,31). However, as the rate and intensity of cavitation is increased the mechanical component is considered to gradually exceed the corrosion effect.

The conditions of our cavitation experiment are indeed of a higher intensity and rate. It is therefore surprising to find such a dependence, of cavitation breakdown rate for coatings, upon the nature of the conductivity and corrosivity of the solution. For example, it is seen from Fig. 16 that the initial rate of cavitation of Al coatings is seen to markedly increase in 3.5 wt% of NaCl compared with DW. A smaller dependence

is seen for Zn, and the ZA shows no significant change. It is additionally seen from Fig. 16 that rolling radically reduces further the cavitation rate of Al, but has no significant effect upon Zn and ZA. It is, therefore, reasonable to assume that porosity has a major influence upon the corrosion component of cavitation for Al. Al produces coatings of far greater porosity than either Zn or ZA; see Fig. 12. Added to this must be the general susceptibility of a coating to localized breakdown. Al is indeed particularly susceptible to pitting in 3.5%wt NaCl solution (32).

The mode of corrosion which is most likely to affect the rate of cavitation behavior of Al coatings is that of crevice corrosion. Crevice corrosion in chloride solutions have been shown to be a special form of pitting behavior (33). The high refreshment rates at the external surface of coatings under cavitation conditions contrast with the stagnant conditions anticipated inside pores. Stagnant conditions may be expected to lead to conditions favorable to pitting inside the pores. Hence Al^{+++} build-up, attracting Cl^- ions into the pores to achieve charge neutrality. Hydrolysis would then result in a lowering of pH, creating a self-buffering solution of saturated hydroxide: (34)

$$Al^{+++} + H_2O = Al(OH)^{2+} + H^+$$

This anodic dissolution would be supported by the cathodic reaction, predominately at the outer regions of pores, due to the high oxygen refreshment rate of the external surface:

$$O_2 + 2H_2O + 4e \rightarrow 4OH^-$$

The internal attack of pores in Al coatings may reasonably be expected to concentrate at the interface of particles, as stresses would be greatest during cavitation at these points of the coating. The brittle nature of the oxide particle-particle interface, would be highly susceptible to stress-assisted attack.

Rolling Al coatings will thus remove a major weakness in the corrosion integrity of these coatings (Fig 19). The effect of corrosion upon the rolled surface may be expected to be centered again at crevices, these being partially sealed pore openings and surface cracks. Sintering, aimed at metallurgically sealing these surface flaws as well as stress annealing the surface would therefore further remove sites of activity from the coating surface. It has previously been demonstrated in Fig. 18 that fewer active sites are opened up in a given time of cavitation, as indicated by the reduced rate of the negative potential shift measured at open circuit.

Zn and ZA are less porous than Al and are likely to be more metallurgically bonded at interparticle boundaries owing to the high vapor pressure of ZnO. The activity of Zn and ZA is seen from Fig. 21 to be greater than Al and only slightly increased with cavitation. Again Fig. 16 demonstrates that Zn and ZA are less prone to corrosion-assisted cavitation erosion.

It is expected that for these coatings, corrosion is of more uniform nature. For Zn it is found that the greatest reduction in the initial rate of erosion is observed for 3.5 %wt NaCl, to be due to sintering (Fig. 22). This is consistent with the higher propensity of cracking found in Zn, as compared with Al. Figure 10 has shown a tendency for higher work hardening rate in DW cavitation to lead to higher cavitation rates at longer times of exposure. It is therefore concluded that the greater effect of sintering in Zn compared with Al is due to stress annealing and crack sintering, should this be possible in the vicinity of the crack tip. Therefore, for metal coatings of lower pitting susceptibility the mechanical component may be expected to far outweigh that of corrosion.

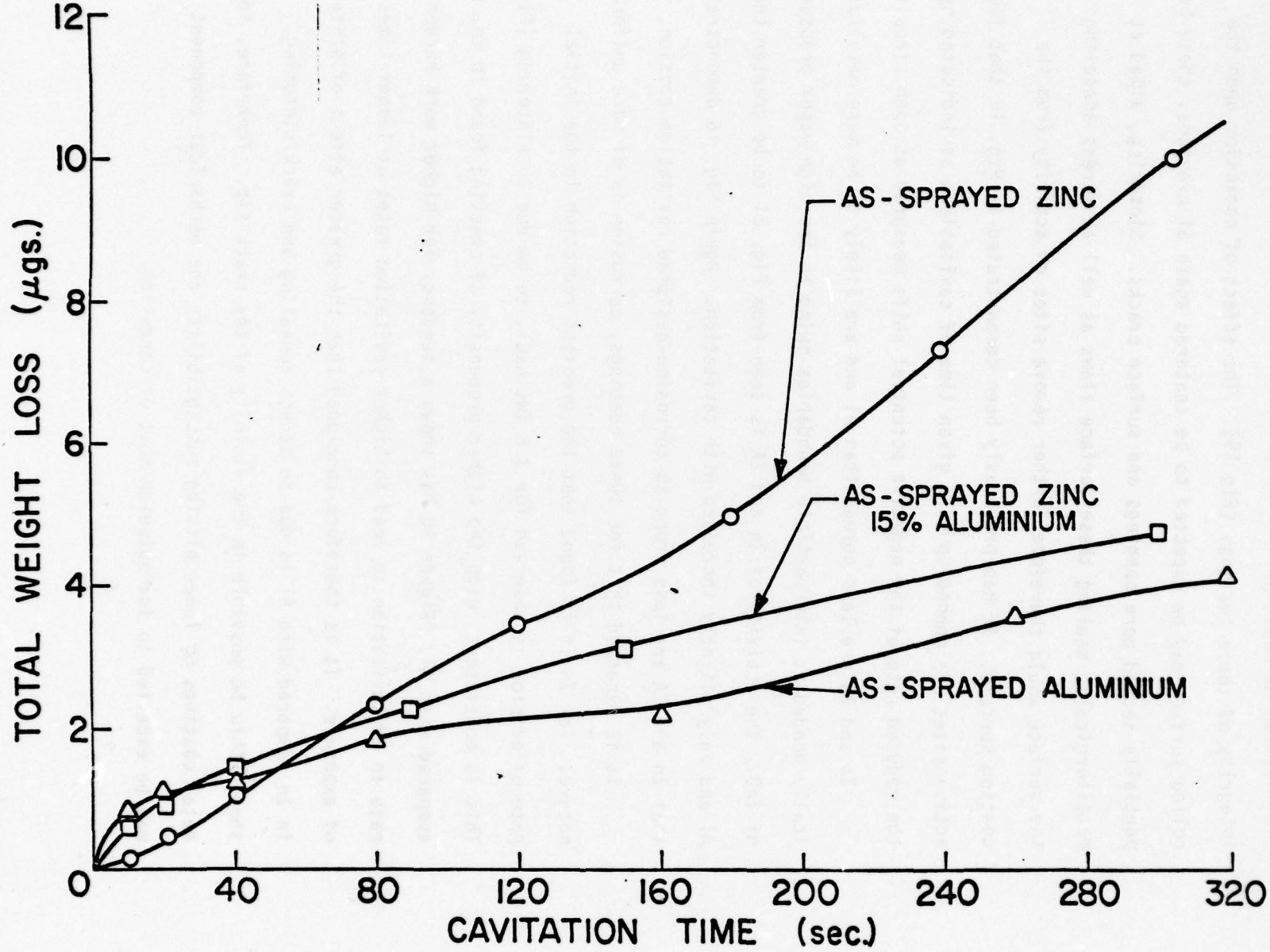
TOTAL WEIGHT LOSS (µgs.)
0
2
4
6
8
10
12
40
80
120
160
200
240
280
320
CAVITATION TIME (sec.)
AS-SPRAYED ZINC
AS-SPRAYED ZINC
15% ALUMINIUM
AS-SPRAYED ALUMINIUM

Fig. 10

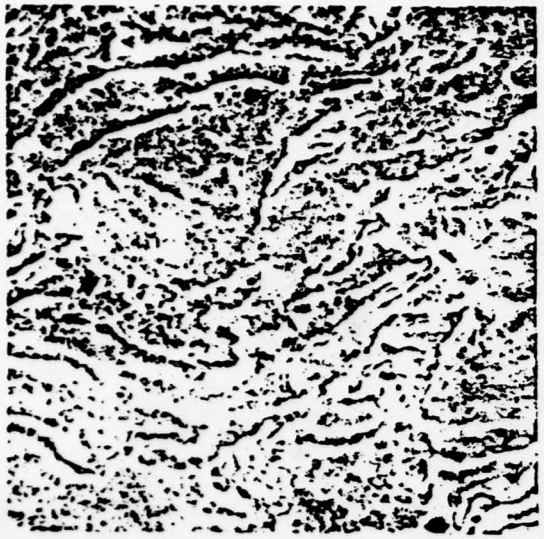

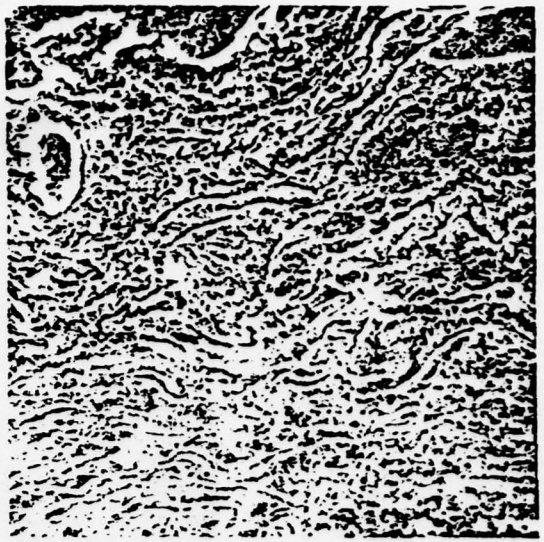

Fig. 11

As-sprayed Zn; side-view, showing dense nature of coating on steel substrate.

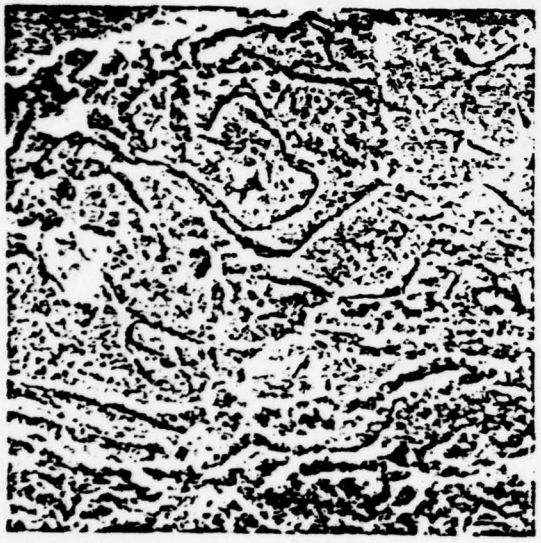

700X

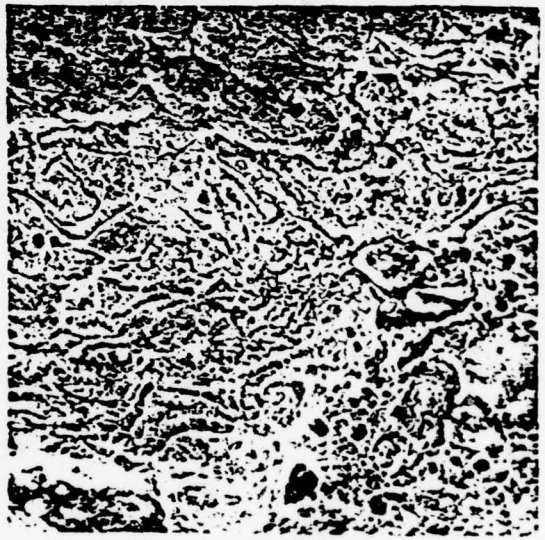

300X

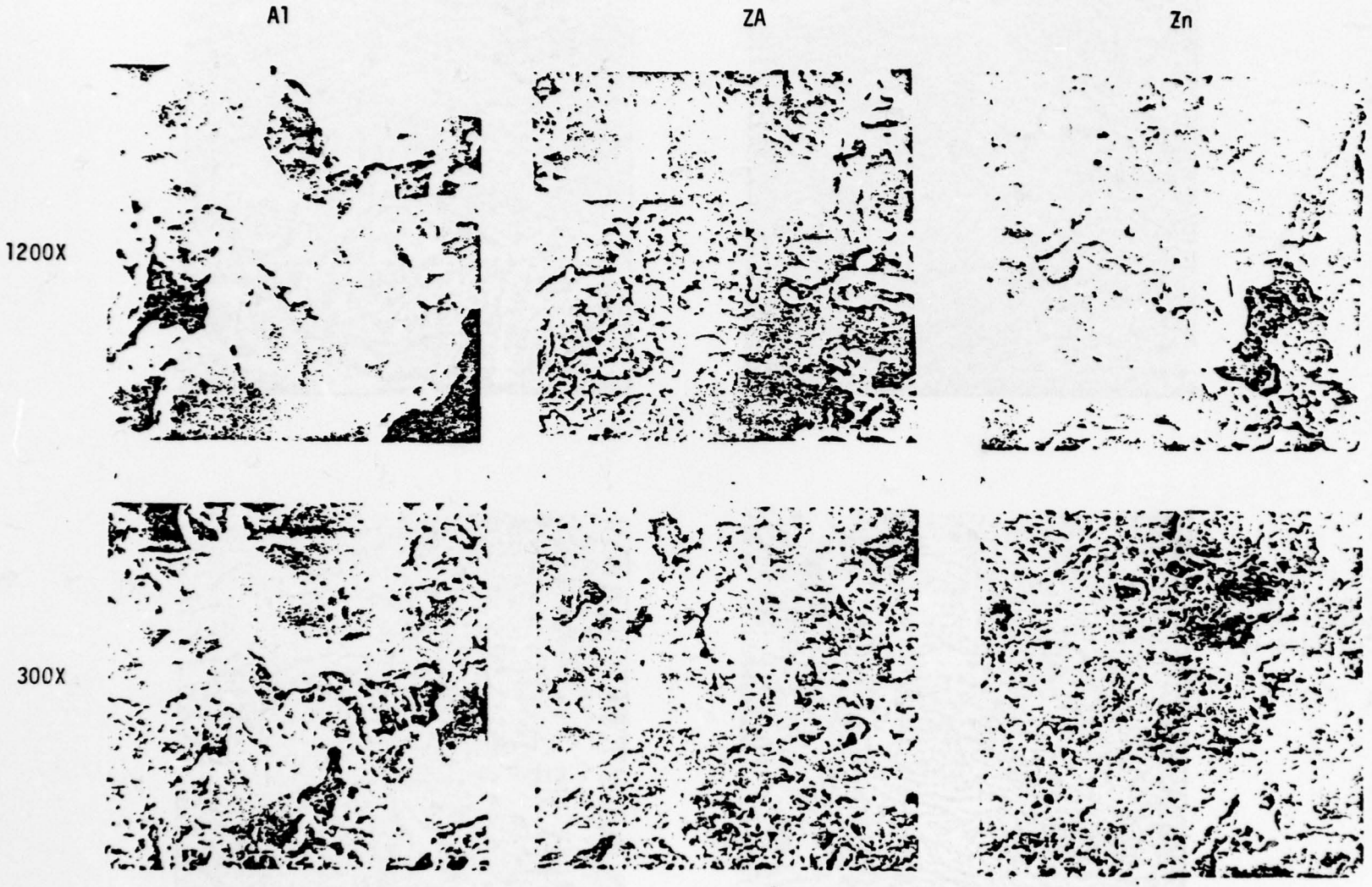

Fig. 12

Top view of the three coatings showing increase in porosity from Al to ZA to Zn

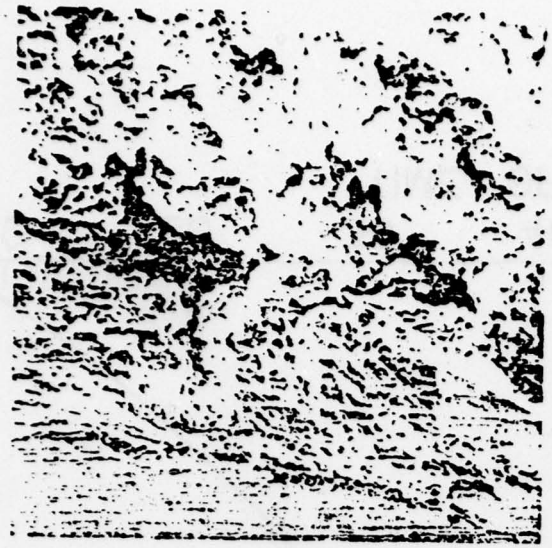

150X

300X

Side-view of as-sprayed Al coating showing high porosity. The roughened steel substrate is at the bottom of the photos.

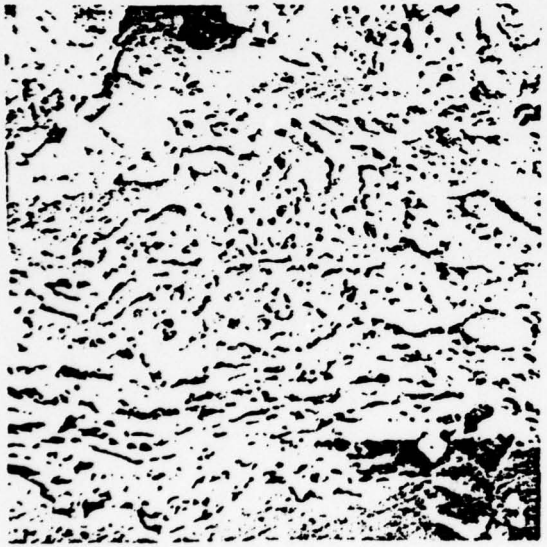

300X

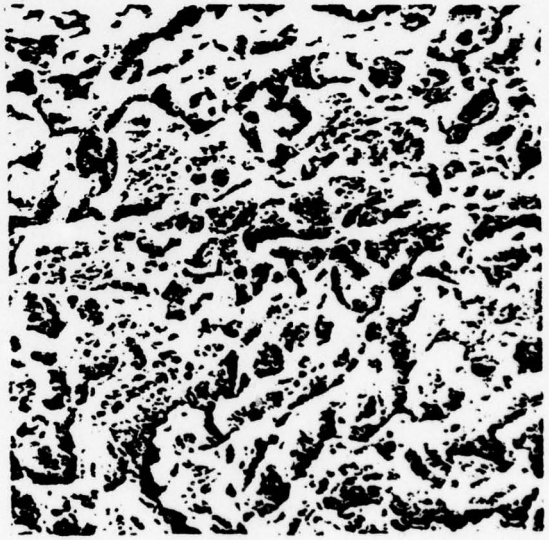

700X

Fig. 13

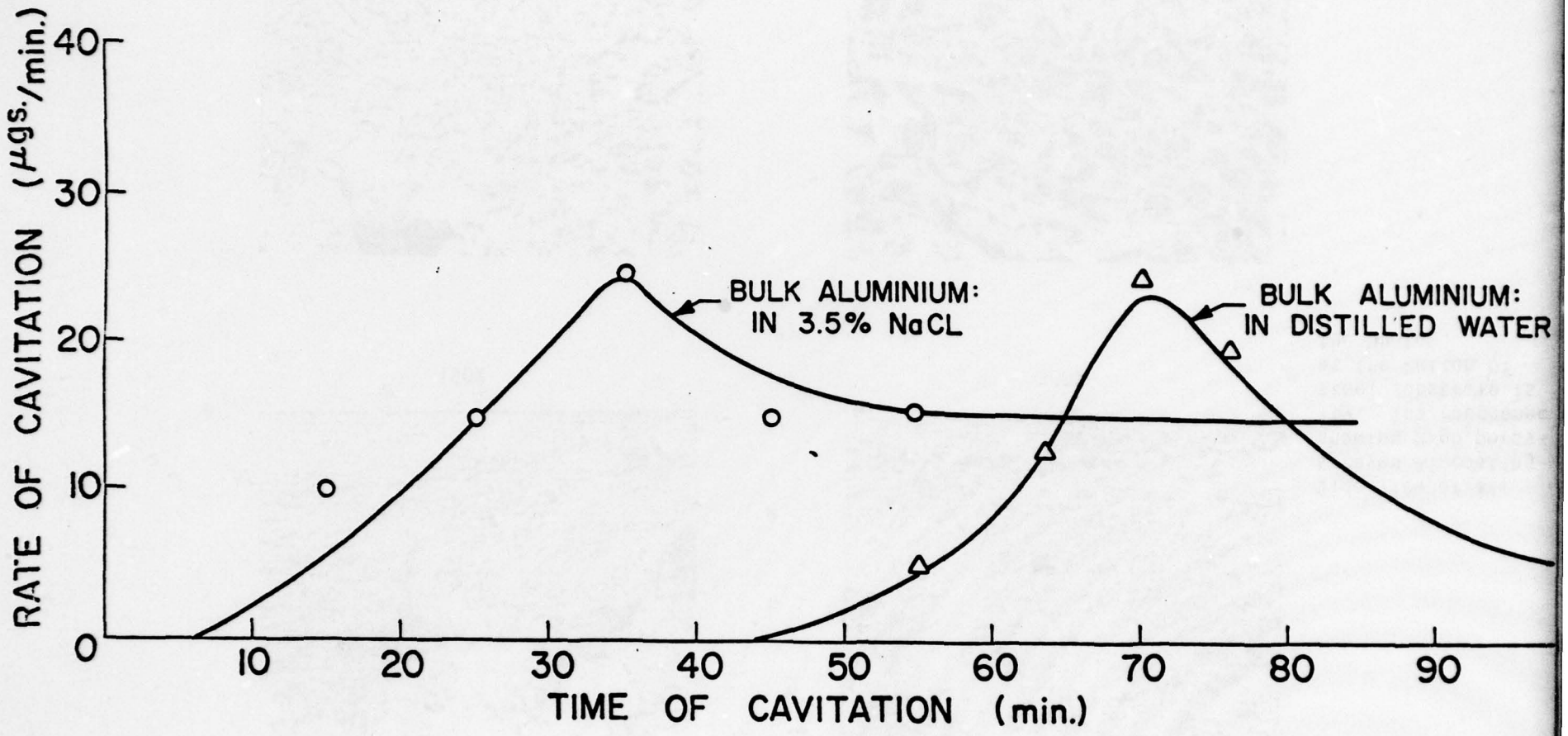
RATE OF CAVITATION (μgs./min.)
40
30
20
10
0
10
20
30
40
50
60
70
80
90
TIME OF CAVITATION (min.)
BULK ALUMINIUM:
IN 3.5% NaCL
BULK ALUMINIUM:
IN DISTILLED WATER

Fig. 14

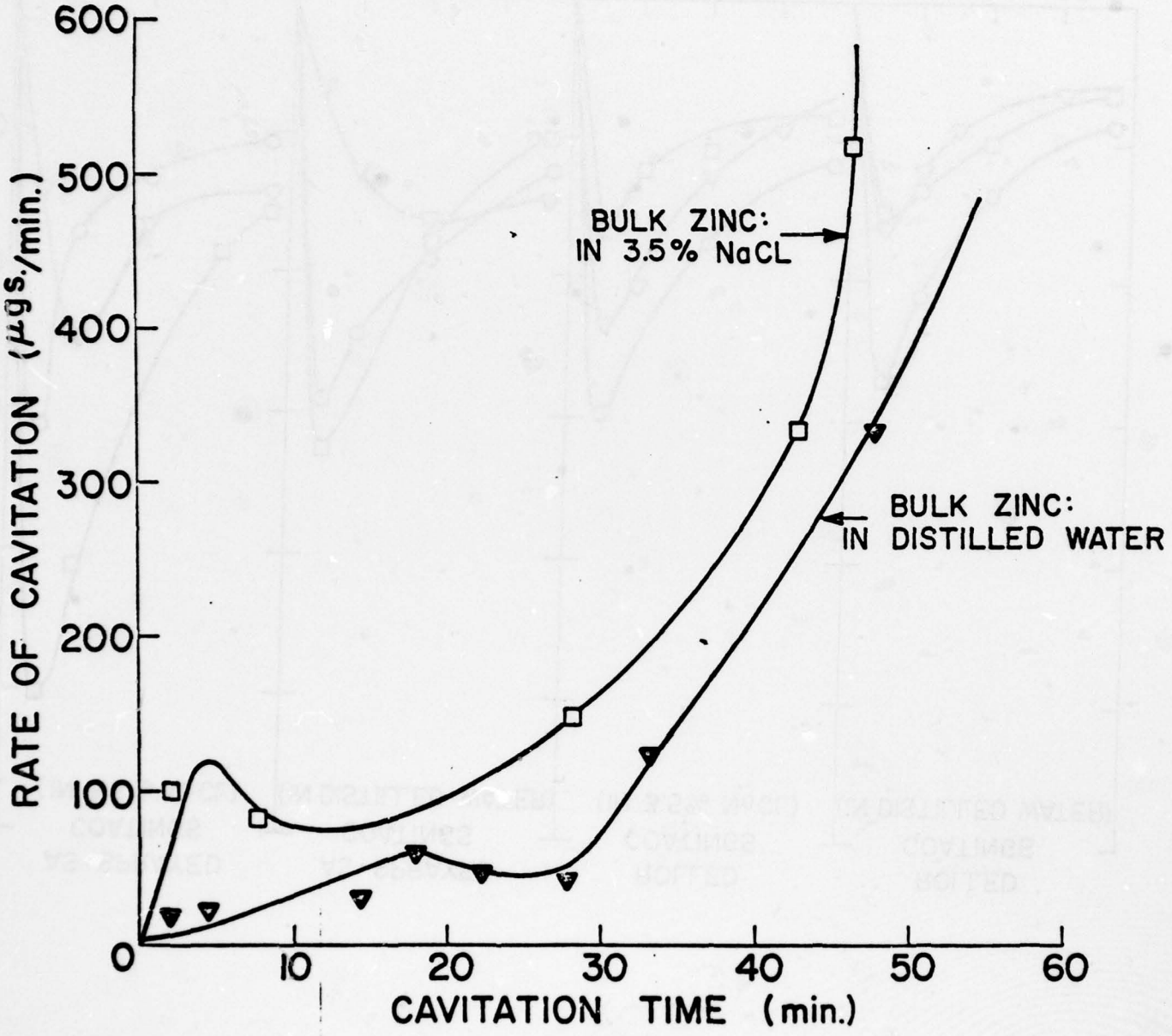
600
500
400
300
200
100
0
RATE OF CAVITATION (μgs./min.)
BULK ZINC:
IN 3.5% NaCL
BULK ZINC:
IN DISTILLED WATER
10
20
30
40
50
60
CAVITATION TIME (min.)

Fig. 75

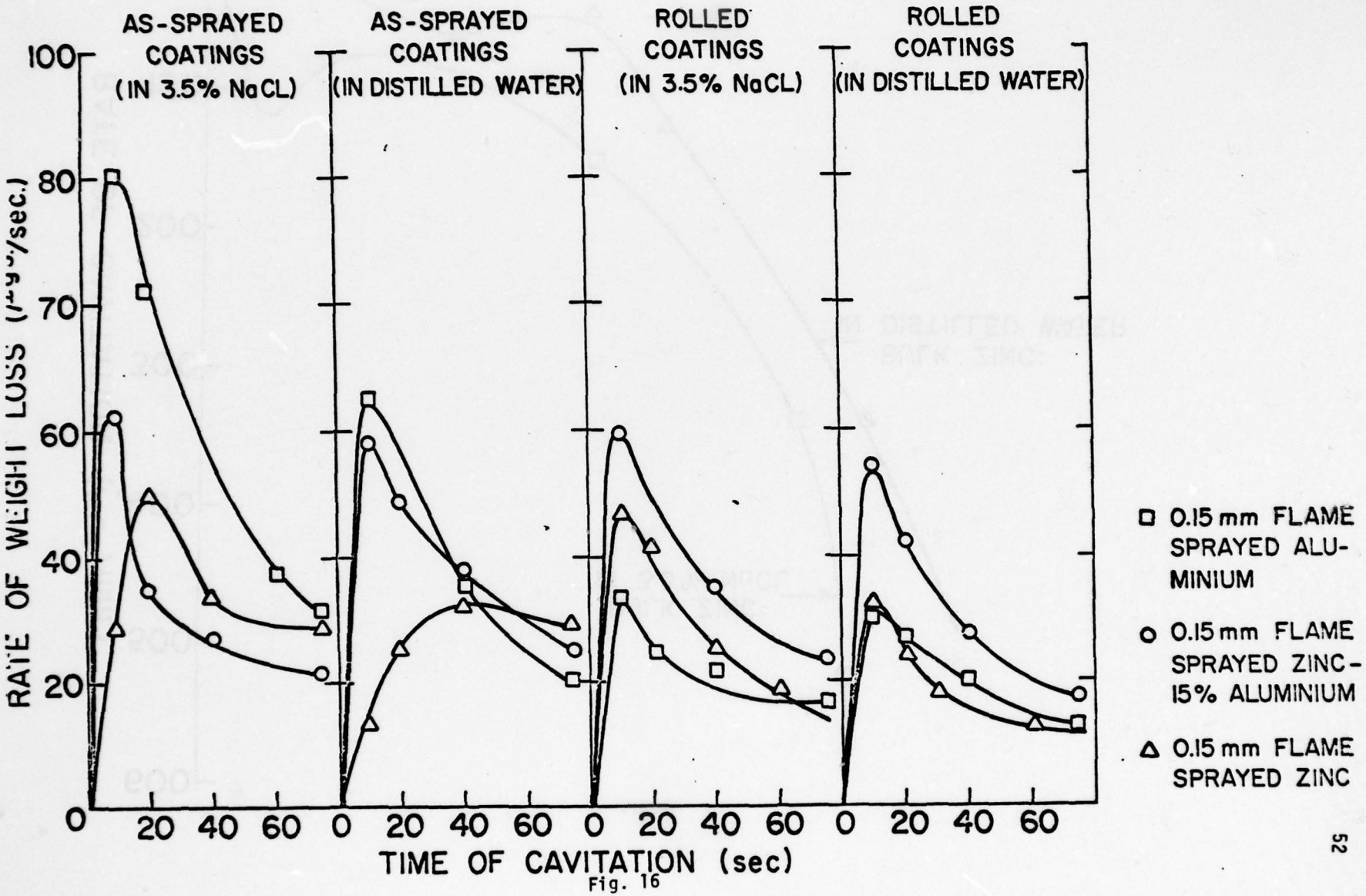
AS-SPRAYED COATINGS (IN 3.5% NaCL)
AS-SPRAYED COATINGS (IN DISTILLED WATER)
ROLLED COATINGS (IN 3.5% NaCL)
ROLLED COATINGS (IN DISTILLED WATER)
RATE OF WEIGHT LOSS (mg/sq.cm/sec.)
100
80
70
60
40
20
0
0 20 40 60 0 20 40 60 0 20 40 60 0 20 40 60
TIME OF CAVITATION (sec)
0.15 mm FLAME SPRAYED ALUMINIUM
0.15 mm FLAME SPRAYED ZINC-15% ALUMINIUM
0.15 mm FLAME SPRAYED ZINC

Fig. 16

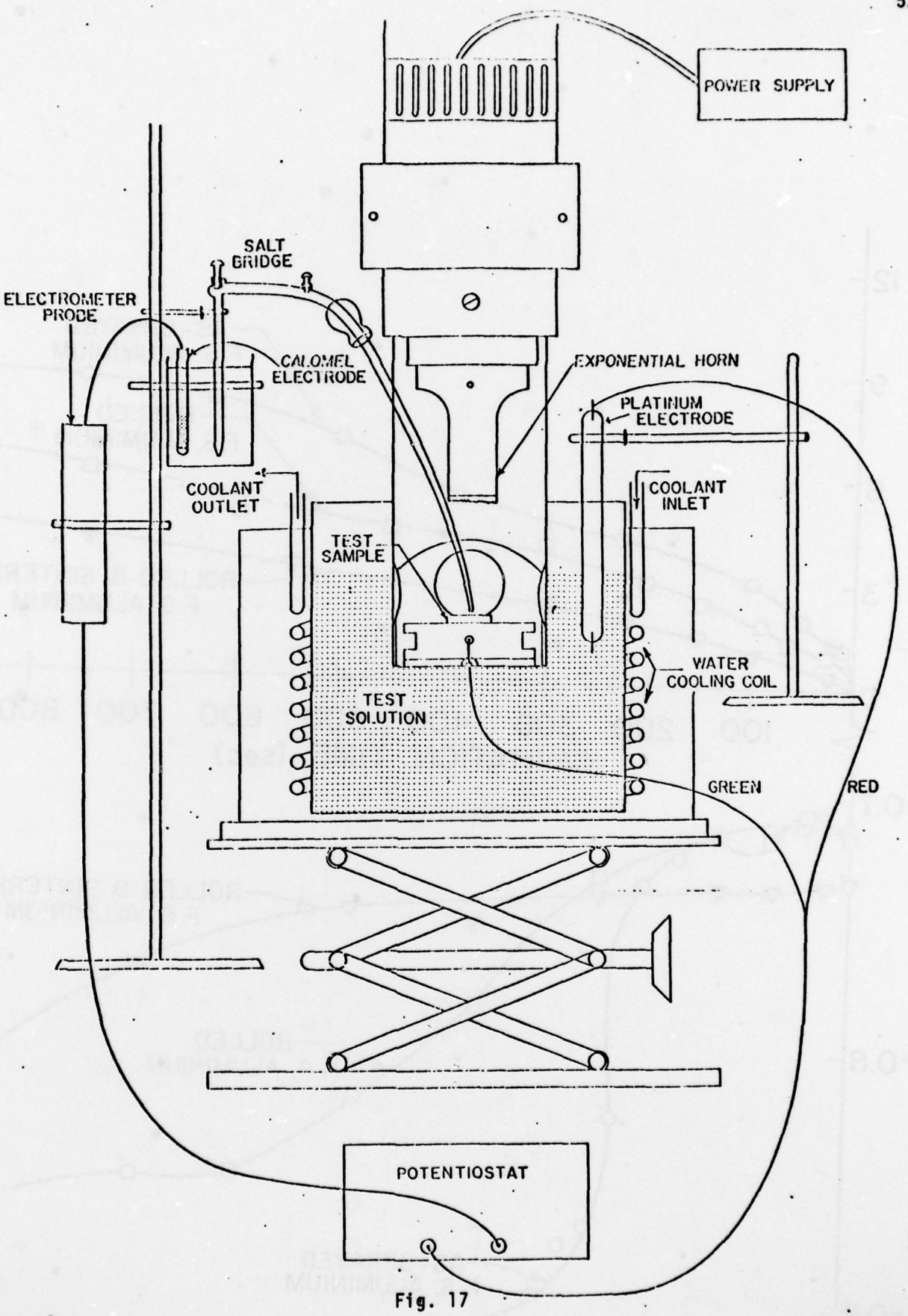
POWER SUPPLY
SALT BRIDGE
ELECTROMETER PROBE
CALOMEL ELECTRODE
EXPONENTIAL HORN
PLATINUM ELECTRODE
COOLANT OUTLET
COOLANT INLET
TEST SAMPLE
WATER COOLING COIL
TEST SOLUTION
GREEN
RED
POTENTIOSTAT

Fig. 17

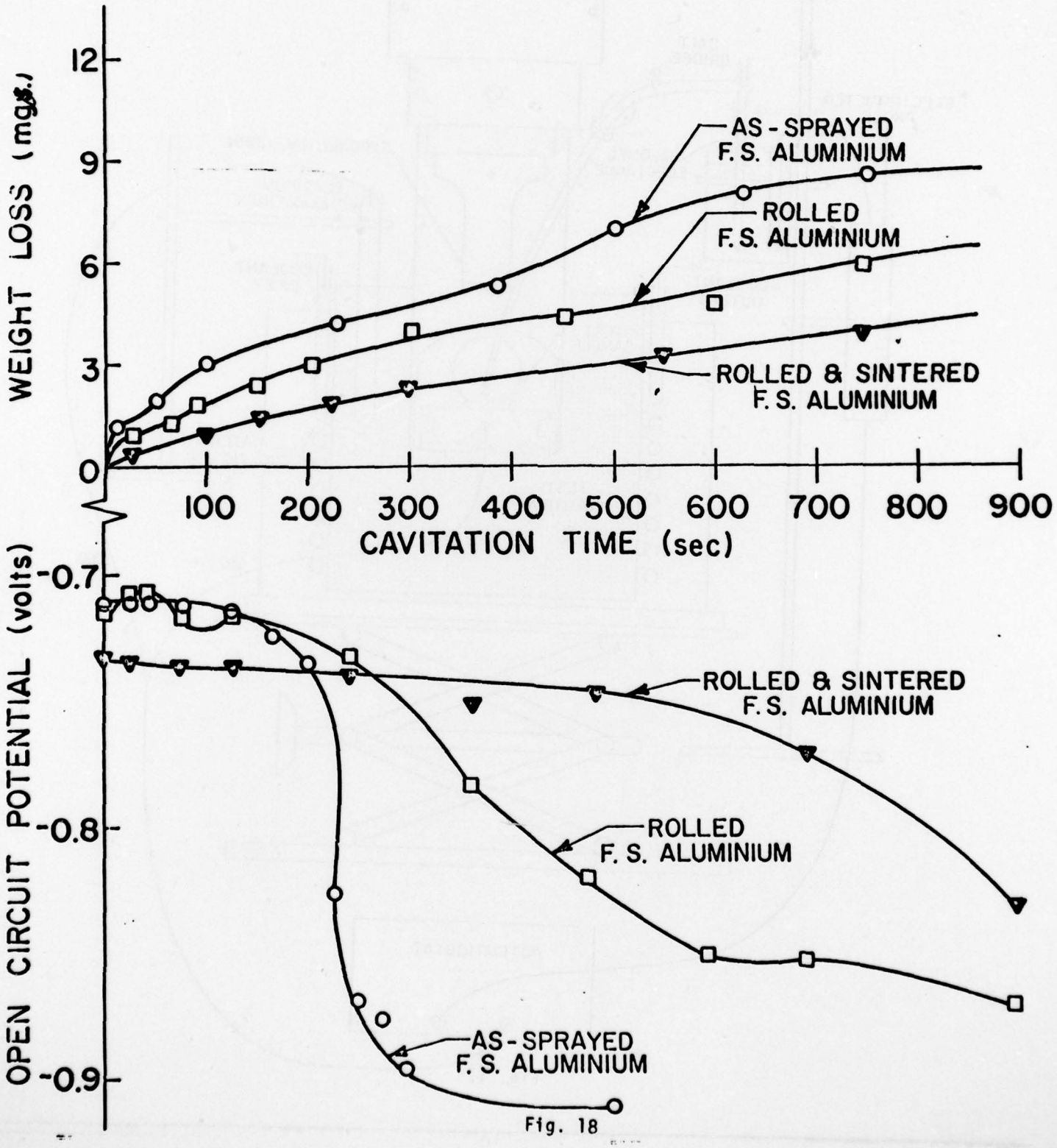
WEIGHT LOSS (mgs.)
12
9
6
3
0
AS - SPRAYED
F. S. ALUMINIUM
ROLLED
F. S. ALUMINIUM
ROLLED & SINTERED
F. S. ALUMINIUM
100
200
300
400
500
600
700
800
900
CAVITATION TIME (sec)
OPEN CIRCUIT POTENTIAL (volts)
-0.7
-0.8
-0.9
ROLLED & SINTERED
F. S. ALUMINIUM
ROLLED
F. S. ALUMINIUM
AS - SPRAYED
F. S. ALUMINIUM

Fig. 18

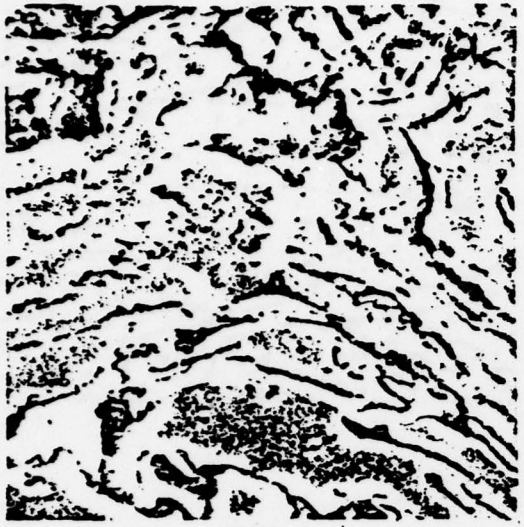

700X

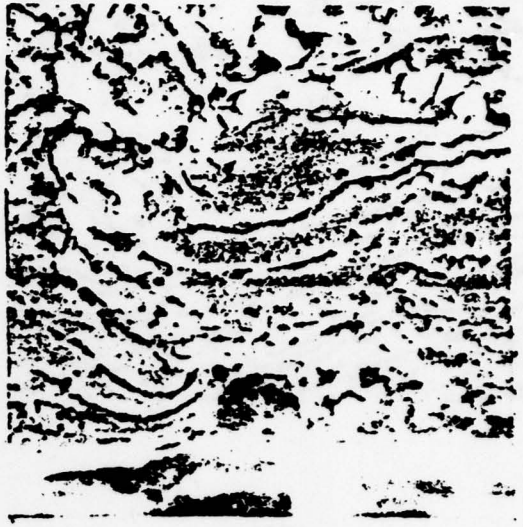

700X

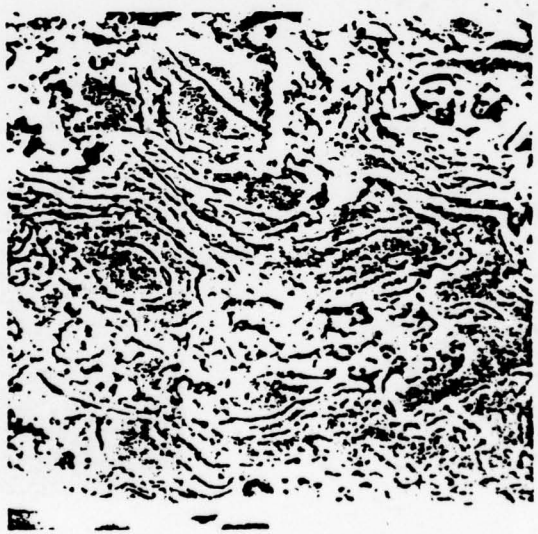

300X

Fig. 19

Sprayed and rolled Al coating on steel

300X

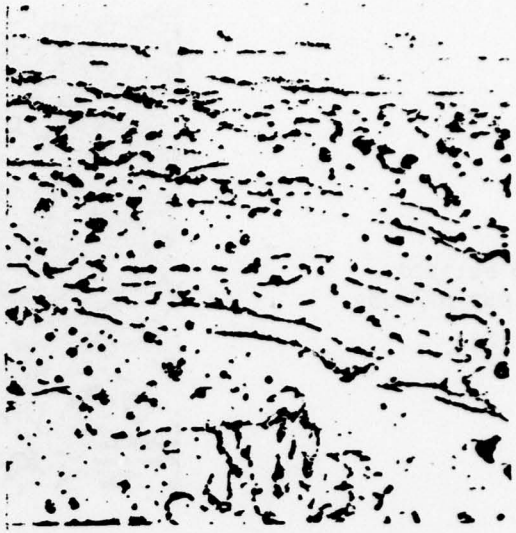

300X

Fig. 20

Sprayed, rolled and sintered Al coating on steel. Sintering was for 3 hrs. at 0.8 T_{MP} of Al.

700X

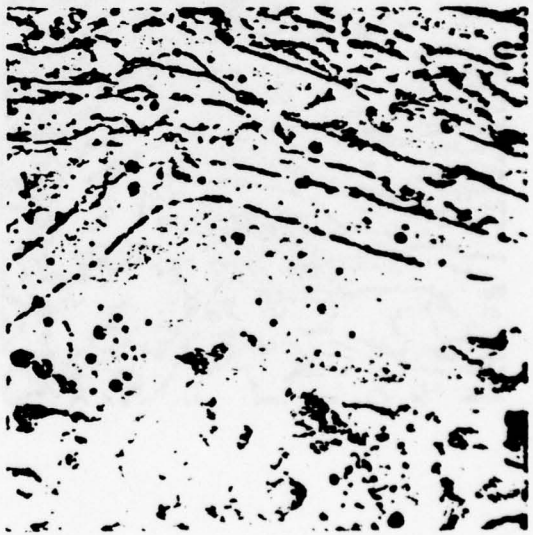

700X

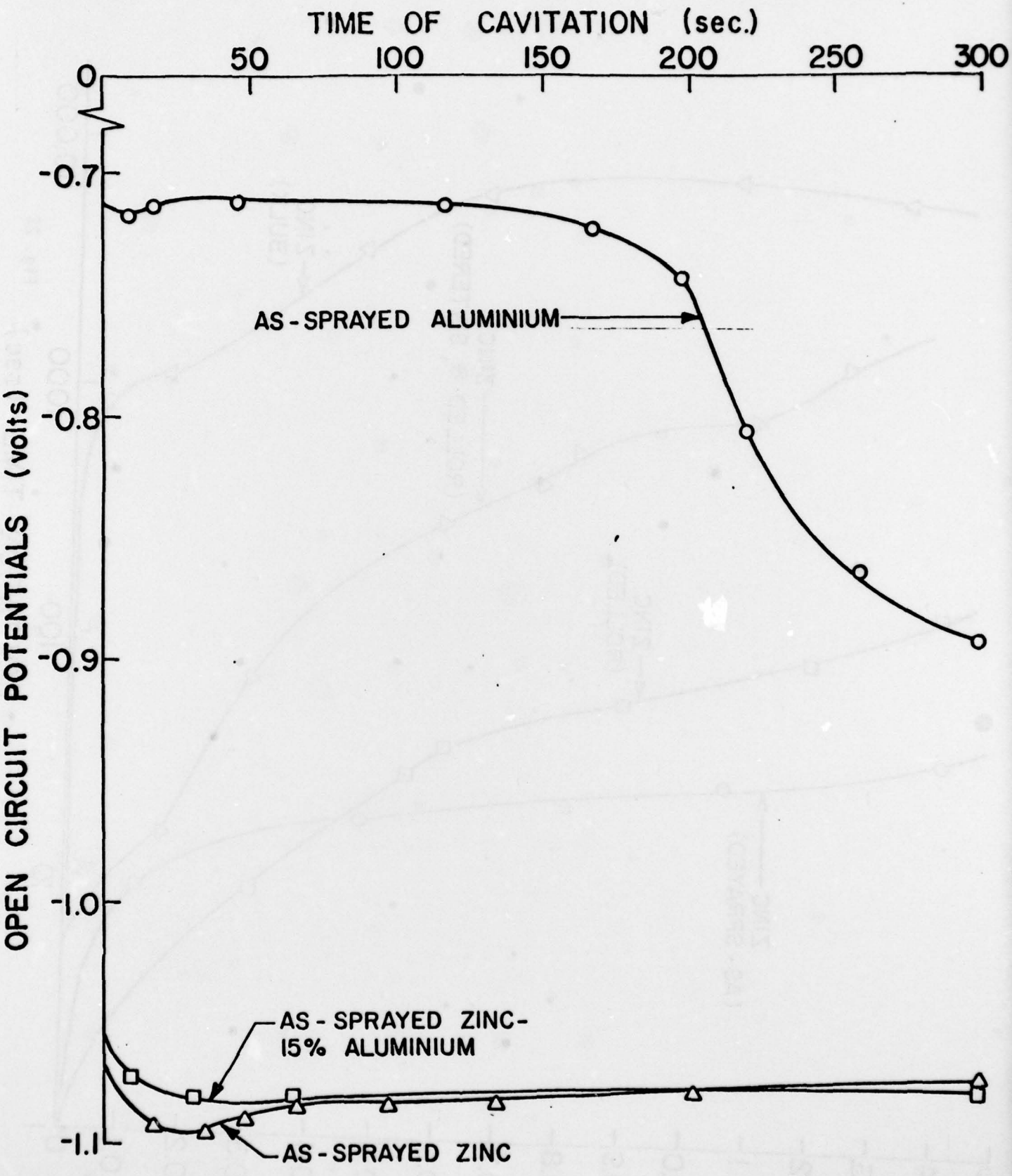
TIME OF CAVITATION (sec.)
0
50
100
150
200
250
300
-0.7
-0.8
-0.9
-1.0
-1.1
OPEN CIRCUIT POTENTIALS (volts)
AS-SPRAYED ALUMINIUM
AS-SPRAYED ZINC-
15% ALUMINIUM
AS-SPRAYED ZINC

Fig. 21

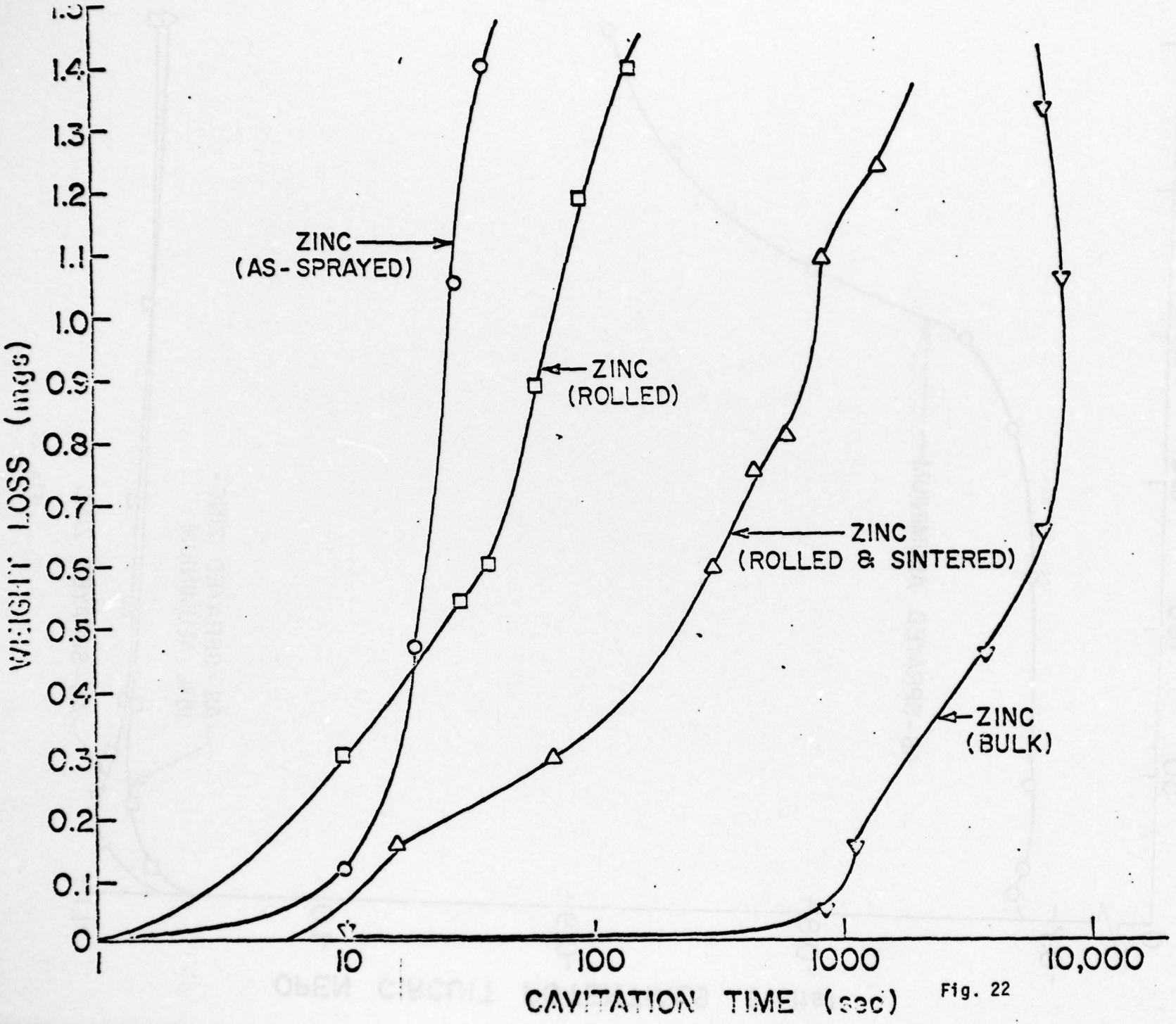
WEIGHT LOSS (mgs)
1.4
1.3
1.2
1.1
1.0
0.9
0.8
0.7
0.6
0.5
0.4
0.3
0.2
0.1
0
ZINC
(AS-SPRAYED)
ZINC
(ROLLED)
ZINC
(ROLLED & SINTERED)
ZINC
(BULK)
1
10
100
1000
10,000
CAVITATION TIME (sec)

Fig. 22

PUBLICATIONS

"Plasma-Spray Coatings - Their Ultramicrostructure", S. Safai and H. Herman; Proc. of the International Conference on Advances in Surface Coating Technology, 1978, British Welding Society, London.

Theses produced during last contract period.

V. Wilms; "The Microstructure of Plasma Sprayed Ceramic Coatings", Ph.D., June, 1978.

S. Safai; "A Microstructural Investigation of Plasma-Sprayed Metal and Oxide Coatings", Ph.D., May, 1979.

J. Vargas; "Thermal-Sprayed Active Coatings for the Marine Protection of Steel", M.S., May, 1979.

Papers to be published:

"AE Emission Study of Plasma-Sprayed Oxides"; S. Safai, K. Ono and H. Herman, Ceramics Bulletin.

"Acoustic Emission Evaluation of Plasma-Sprayed Oxide Coatings", S. Safai, K. Ono and H. Herman, to be presented at the International Metallurgical Coatings Conference, San Diego, CALIF. April, 1979. To be published, Thin Solid Films.

REFERENCES

1. American Welding Society Corrosion Tests of Metallized Coated Steels, 12 Year Report, AWS Report #C2.11-67 (1967).

2. "Corrosion Tests of Flame Sprayed Coated Steels", American Welding Society 19 Year Report, AWS Report #C2.14-74 (1974).

3. "The Response of Coated Steels to Cavitation in Corrosive Environments", 1st Annual Report to ONR on Contract No. N00014-75-C-1018, May, 1976.

4. ibid, 2nd Annual Report, May, 1977.

5. ibid, 3rd Annual Report, May, 1978.

6. Das, A.R.; "Liquid-Solid Transformation Kinetics in Aluminum Oxide", Ph.D. Thesis; UCRL, Berkeley, Ca. (July 15, 1964).

7. Dragoo, A.L. and Diamond, J.J.; J. Amer. Ceram. Soc. 50, 568 (1967).

8. V. Wilms and H. Herman, "Plasma Spraying of Al_2O_3 and Al_2O_3-Y_2O_3", Thin Solid Films, 39, 251-262 (1976).

9. S. Safai and H. Herman, "Microstructural Investigation of Plasma-Sprayed Aluminum Coatings", Thin Solid Films, 45, 295-207 (1977).

10. Krepski, R.P.; "The Liquid-Quenching of Laser-Melted Oxides", Master degree Thesis, SUNY at Stony Brook, N.Y., Aug. 1975.

11. Lippens, B.C. and DeBoer, J.H.; Acta Cryst. 17, 1312 (1964).

12. S. Safai, "A Microstructural Investigation of Plasma-Sprayed Metal and Oxide Coatings", Ph.D., May, 1979.

13. Bagley, R.D., "Effects of impurities on the sintering of alumina", Ph.D. thesis, Univ. of Utah (1964).

14. Winkler, E.R. and Cutler, I.B., "Ceramics microstructures", Ed. R.M. Fulrath and J.A. Pask; J. Wiley & Sons, (1966), pp. 267-276.

15. McKee, W.D., Jr. and Aleshin, E., J. Amer. Ceram. Soc. 46, 54 (1903).

16. Gani, M.S.J. and McPherson, R., J. Australian Ceram. Soc. 8, 65 (1972).

17. Tkachenko, Uy. G. et al., Soviet Powder Metallurgy and Metal Ceramics 16(6), 454 (1977).

18. Lange, S.M., et al., J. Research of the National Bureau of Standards, 48 (4), 298 (Apr. 1952).

19. Bailey, J.T. and Russell, Jr., Trans. Br. Ceram. Soc. 68(4), 159 (1969).

20. Rasmusson, J.J., et al., J. Amer. Ceram. Soc., 48, 146 (1965).

21. Garvie, R.C., "Zirconium dioxide and some of its binary Systems", in High Temperature Oxides, Ed. by A.M. Alper, 1970, pp. 118-167.

22. Suzuki, T. and Anthony, A.M., Mat. Res. Bull. 9, 745 (1974).

23. Takamori, T. and Roy, R., Advances in Nucleation and Crystallization in Glasses", Ed. by L.L. Hench and S.W. Freiman, Amer. Ceram. Soc. 1971, pp. 176-182.

24. Takamori, T. and Roy, R. and McCarthy, J., Mat. Res. Bull. 5, 529 (1970).

25. Anderson, S. et al., Acta Chemica Scandinavica 11, 1641-1652 and 1653-1657 (1957).

26. Bursill, L.A. and Hyde, B.G., Phil. Mag. 20, 347 (1960). Also 23, 3 (1970).

27. Anderson, J.S. and Hyde, B.G., J. Phys. Chem. Solids, 28, 1393 (1967).

28. Minnear, W.P. and Bradt, R.C., J. Amer. Ceram. Soc. 60, 458 (1977).

29. S. Safai and H. Herman, "Plasma-Sprayed Coatings: Their Ultra-Microstructure", Proceedings, International Conference on Advances in Surface Coating Technology", 13-15 Feb., 1978, London, The Welding Institute, Britain, 1978.

30. M.S. Plesset, Corrosion, 18, No. 5, p. 181 (1962).

31. H.S. Preiser and B. G. Tytell, Corrosion 17, No. 11, p. 107 (1961).

32. H.P. Leckie and H.H. Uhlig, J. Electrochem. Soc., 113, p. 1262 (1966).

33. Z. Szklarska-Smialowska and J. Mankonski, Corrosion Sci., 18, p. 953, (1978).

34. I.L. Rosenfeld and I.K. Marshakov, Corrosion, 20, 115 (1964).